Boston University

OpenBU http://open.bu.edu

Boston University Theses & Dissertations Dissertations and Theses (1964-2011)

2010

Electrothermally actuated terahertz metamaterial

https://hdl.handle.net/2144/34955

Downloaded from DSpace Repository, DSpace Institution's institutional repository

BOSTON UNIVERSITY

COLLEGE OF ENGINEERING

Thesis

ELECTROTHERMALLY ACTUATED TERAHERTZ METAMATERIAL

by

Mehmet Saadeddin OZTURK

B.S., Kadir Has University, 2006

Submitted in partial fulfillment of the

requirements for the degree of

Master of Science

2010

Approved by

First Reader 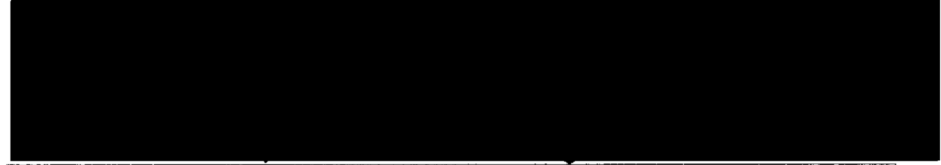

Xin Zhang, PhD
Associate Professor of Mechanical Engineering

Second Reader 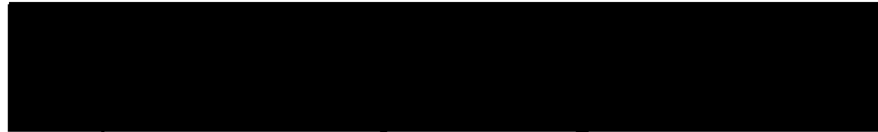

Richard D. Averitt, PhD
Associate Professor of Physics Department

Third Reader 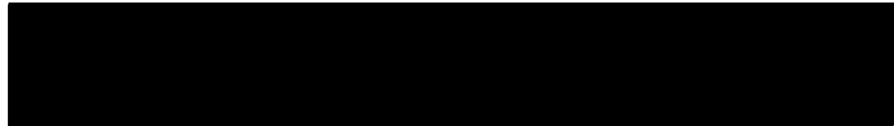

Hatice Altug, PhD
Assistant Professor of Electrical and Computer Science Engineering

Acknowledgments

First and foremost, I would like to thank professor Zhang. She provided her full support through out these two years. She has been a great mentor that she helped me to keep my self in the track, motivated and focused.

I want to thank professor Averitt. He trusted me and provided me his full technical and motivational support. I felt a huge motivation and encouragement after every single discussion we had together.

It was a great pleasure and honor for me making research under their supervision. I'm looking forward to working with them in the future.

I would like to thank professor Altug for being my committee member and sharing her time with me in her busy schedule.

This brings me to thank Kebin and Drew. I have learned almost everything in terms of fabrication from Kebin. Drew has been open for all my questions in terms of physics. His support once even extended to a Sunday afternoon lab work. This project would not be possible without their support and informative discussions.

I want to thank Tiger and Ken for having beneficial discussions and providing their experience in fabrication with me.

I want to thank Travis for letting me used his 2 inch wafers, wafer box, sample holders and many lab consumer products and also being a lab mate during late night work in the clean room. I also want to thank Yiling, being like an older brother for whole group and helping me to meet with the rest of the group.

I would like to thank all the Laboratory for Microsystems Technology and Multifunctional Material Spectroscopy Laboratory graduates and for their contributions.

I want to thank Abdulkadir and Ahmet for being a patient roommate espe-

cially in the last period of thesis writing. I could not have over come hard times without their friendship.

I would like to thank Engin, Huseyin and Alket for cleaning up my grammar in the thesis and creating a friendly environment in the office.

Of course, I would like to thank my family for their continues support even though they are thousands of miles away. All my educational work is just a couple of stones on the base that they prepared for me.

ELECTROTHERMALLY ACTUATED TERAHERTZ METAMATERIAL

Mehmet Saadeddin OZTURK

ABSTRACT

Microelectromechanical Systems (MEMS) have been adapted from Integrated Circuit (IC) technology. MEMS enable fabrication of devices size from a few microns to hundreds of microns. This scale is also a proper scale for Terahertz (THz) metamaterials (MM), which are designed for building homogeneous mediums. Our study aims to demonstrate an operating device which is designed by using mechanical and electromagnetic principles, fabricated by MEMS technology.

MEMS actuator and electromagnetic resonator are the two main parts of our device which is called Electrothermally Actuated Metamaterial (ETAMM). Mechanical actuator is realized by using conventional photolithography techniques and THz Time Domain Spectroscopy (TDS) is used for excitation and detection of the resonator. This project is a contribution to the active THz MM devices of which main purpose is to control the optical property by an external stimuli.

We aimed to fabricate a tunable THz Metamaterial device. The device is comprised of two mirrored Split Ring Resonator (mSRR) with a certain resonant frequency. Resonance frequency is tuned by electrothermal actuation. As a novel approach, mSRR itself is used as an actuator. Devices are connected to each other through electrodes. They make the current flow through an array and this flow leads to joule heating by causing a thermal expansion of the device. This elastic deformation of the device results as in an out of plane buckling and changes the distance between mSRR and bare silicon substrate.

In the electromagnetic part of the mechanism; the change in distance, caused

by thermal expansion, alters the effective dielectric constant within the gap between the structure and the substrate. Dielectric constant in the gap is the main parameter for resonance frequency, for this reason we chose it as a tuning parameter of the device.

In the final analysis, ETAMM utilizes the change in the dielectric constant to alter the resonance frequency. Our device delivered 6 GHz resonance frequency shift as a response to an applied voltage of 5.7V on the device.

Contents

1 Introduction **1**

2 Designing Active Metamaterial **4**

2.1 Mechanical Design 4

2.1.1 Bending Mechanism 4

2.1.2 Bar Buckling 7

2.1.3 Heat Transfer Modal 12

2.1.4 Electrothermal Heating 14

2.1.5 Finite Element Analysis of Mechanical Modal 15

2.2 Electromagnetic Design 18

2.2.1 Effective Medium Theory 18

2.2.2 Split Ring Resonators 21

3 Fabrication **34**

3.1 Fabrication Steps 34

4 Measurement **42**

4.1 Electrothermal 42

4.1.1 Measurement Results 42

4.2 Terahertz Time Domain Spectroscopy 46

4.2.1 THz Time Domain Spectroscopy Setup 46

4.2.2 Measurement Result 46

References **49**

Curriculum Vitae **51**

List of Figures

2·1 Beam and spring relation 5

2·2 Tension and Compression Representation on a beam 6

2·3 Shape Function of a doubly pinned beam 11

2·4 Bending moment of a doubly pinned beam 11

2·5 Shape Function of different modes 12

2·6 Voltage distribution on the structure 17

2·7 Temperature distribution of the device 17

2·8 z-Displacement is shown for a thermal expansion 18

2·9 Capacitor 20

2·10 Circuit schematic of a capacitor (C) series in an inductor (L) . . . 22

2·11 SRR structure and its electrical circuit equivalence 23

2·12 Mirrored Split Ring Resonator field configuration 24

2·13 Equivalent circuit of mirrored SRR structure has two parallel inductors and one capacitor is shunted to them. 25

2·14 Due to a potential difference between two ends of the device, there is a current flow. This current flow causes a resistive heating . . . 27

2·15 A capacitor modal with E-Field lines between conductor plates. Field lines passing through both air and substrate 28

2·16 E-Field is on x-axis, H-Field is on y-axis, the wave propagates into the plane 29

2·17 Thick line (red in online copy) is the transmission data of mSRR with no rotation, thin line (gray in the online copy) is the transmission data with the device has 90 degree clockwise rotation . . 29

2·18 Red line (left curve) indicates the transmission when g=1, green line (right curve) indicates transmission when g=2. This simulation result shows nearly 40 GHz resonance shift for 1micron deflection. Height of the device is 1 micron over the substrate before deflection. g is the gap distance between the structure and the substrate 30

2·19 Red line (left curve) indicates the transmission when g=2.1, green line (right curve) indicates transmission when g=2.9. This simulation shows about 15 GHz resonance shift for 0.8 micron. Height of the device is 1 micron over the substrate before deflection (g is the gap distance between the structure and the substrate) 31

2·20 Resonance shift for a beam length of 50 μm. E-Field is on x-axis, H-Field is on y-axis, the wave propagates into the plane 32

2·21 Resonance shift for a beam length of 100 μm. E-Field is on x-axis, H-Field is on y-axis, the wave propagates into the plane 32

2·22 Resonance shift for a beam length of 150 μm. E-Field is on x-axis, H-Field is on y-axis, the wave propagates into the plane 33

3·1 Ti/Au is deposited as seed layer with E-Beam Evaporation 35

3·2 Sacrificial layer is coated and Second Au layer is deposited 35

3·3 S1818 photoresist is coated and patterned. Cu is electroplating for the main structure 36

3·4 The last Au is deposited on the electroplated Cu structure 36

3·5 Released structure after CPD process 37

3·6 Suspending beam is about 1 micron above the substrate 38

3·7 Top view of the released structure 38

3·8 Scanning Electron Microscopy image of a suspending array 39

3·9 Damaged structure after sonication 40

3·10 Suspending array after sonication 40

3·11 A:CO_2 liquid inlet valve, B:Air outlet, B:Pressure Display, C: Temperature Display, D: High pressure chamber, also heated up by circulating hot water within the cylinder 41

4·1 2D profile, x and y axis projections of the structure at 0V applied 43

4·2 2D profile, x axis projection of the structure at 1V applied 44

4·3 2D profile, x axis projection of the structure at 2V applied 44

4·4 2D profile, x axis projection of the structure at 3V applied 45

4·5 2D profile, x axis projection of the structure at 4V applied 45

4·6 2D profile, x axis projection of the structure at 5V applied 45

4·7 THz Time Domain Spectroscopy Setup 47

4·8 Resonance Frequency Tuning of ETAMM by applied voltage: (a) 0 – 0.5 THz Range; and (b) Close-up graph of the view 1. Around 6 GHz resonance shift 48

List of Abbreviations

BC	....	Boundary Conditions
CPD	....	Critical Point Dryer
DC	....	Direct Current
EM	....	Electro Magnetic
ETAMM	....	Electrothermally Actuated Terahertz Metamaterial
GaAs	....	Gallium Arsenide
IC	....	Integrated Circuit
MEMS	....	Microelectromechanical Systems
MM	....	Metamaterial
mSRR	....	Mirrored Split Ring Resonator
SEM	....	Scanning Electron Microscopy
SRR	....	Split Ring Resonator
TDS	....	Time Domain Spectroscopy
THz	....	Terahertz

Chapter 1

Introduction

Microelectromechanical Systems ($MEMS$) are adapted from well developed Integrated Circuit (IC) technology. MEMS has provided a successful research area in terms of miniaturizing macro scale devices, like gyroscopes, micro turbines, ink jet printers, as well as building its own focus areas such as image sensors, accelerometers. Lately, MEMS technology is integrated with a new area called Terahertz (THz) Science.

THz range of electromagnetic (EM) spectrum has been studied since the demonstration of the first metamaterial for GHz range (Smith et al., 2000). Recently research effort has shifted to THz range. MEMS play an important role for realizing devices in this range, because of the perfect match between the scale of device size, possible with MEMS technology and required device size to operate in THz range.

The purpose of THz science is to fill the gap in electromagnetic spectrum (0.1 THz - 100 THz) by developing proper devices. THz spectrum is getting functionalized with the help of rapid development of metamaterials in this range. Because most of the natural materials do not operate in THz regime. Therefore a special material is needed in order to use this gap. Metamaterials is realized with *effective medium theory.*

A material with a unit cell size (a) much smaller than wavelength of the incident light (λ) can be fabricated. According to effective medium theory, if the unit cell size satisfies the mentioned condition, $refraction$ phenomena dominates over

diffraction and *scattering* and the artificial material behaves as a homogeneous medium.

Combining MEMS technology and metamaterial phenomena opens a new research area called *active THz metamaterial.* Compatibility of these two makes it possible to produce materials that can change its electromagnetic property with an applied external stimuli. This concept has been developed by Padilla et.al. (Padilla et al., 2006).

Four of the active MM device papers will be discussed here.

The first device was demonstrated in 2006 by Padilla et.al. (Padilla et al., 2006) also published a paper about switching a propagating THz signal by photoexcitation of charge carriers in the semi-insulating GaAs substrate. Main improvement over (Chen et al., 2006) is faster switching (*femtosecond pulses*) of the first mode resonance frequency.

In the same year (2006) by Chen et.al. A device is comprised of oppositely combined split ring resonator (*SRR*) in order to cancel any magnetic response. Electrically coupled structure provides a resonance frequency. The device has been designed in a way that works as a Schottky diode. An increasing gate voltage (0-16 V) enlarges the depletion region and decreases conductivity. This will increase the capacitance which will directly affect the strength of the resonance characteristic of the device. Chen et.al. stated 10 KHz modulation frequency.

Ultrafast modulation was realized by Chen et.al in 2007. They demonstrated a switching by photogeneration of carriers in GaAs substrate around 10 picosecond (Chen et al., 2007).

Another study has been published by Paul et.al in 2009. The main improvement is the operation of the device independently from incident wave polarization. They used a cross structure device, which makes the device insensitive to polarization. They demonstrated a modulating frequency around 100 KHz (Paul et al., 2009).

We introduced a new approach for tuning THz Metamaterials. Our aim is to tune resonance frequency of the device with an electrothermal stimuli. There are two new approaches in this design: first, using electrothermal actuation mechanism for tuning resonance frequency and second, moving the resonance up and down in a certain frequency range. Electrothermally actuated THz Metamaterial operates both as a mechanical actuator and as an electromagnetic Electromagnetic (EM) resonator.

Mechanical actuation is realized by the resistive heating phenomena. A double pinned suspending beam is heated and as a result it expands and buckles up. Changing the distance between the suspending beam and the substrate changes the capacitance of the device . In measurements, we obtain approximately 1 μm out of plane buckling. A 6 GHz frequency shift is obtained for 0 Volt to 5.7 Volt applied potential on the device. Our measurements are conducted in ambient environment. By putting the device in a vacuum and also minimizing fabrication imperfections, the response can easily be improved.

Chapter 2

Designing Active Metamaterial

Standard beam bending under no constraints will be investigated in the first part. Then fixed-fixed beam bending characteristics will be examined.

After mechanical theory, heat transfer phenomena will be explained briefly. Heat transfer model also will be shown in this section.

Next step for designing the device will establish an electrothermal modal of the device including relation between applied DC voltage and temperature change.

In the last section electromagnetic modal of the system and simulation results will be examined.

2.1 Mechanical Design

2.1.1 Bending Mechanism

Under an axial load, a beam will behave like a spring. A beam has a width w, a thickness t and a length ℓ. Axial stress for this beam is defined as an applied force F over unit cross sectional area A.

$$\sigma = \frac{F}{A} = \frac{F}{wt} \tag{2.1}$$

So the strain on the beam is;

$$\epsilon = \frac{\sigma}{E} = \frac{F}{Ewt} \tag{2.2}$$

where E is the *Young's Modulus*. Length change of the beam is represented

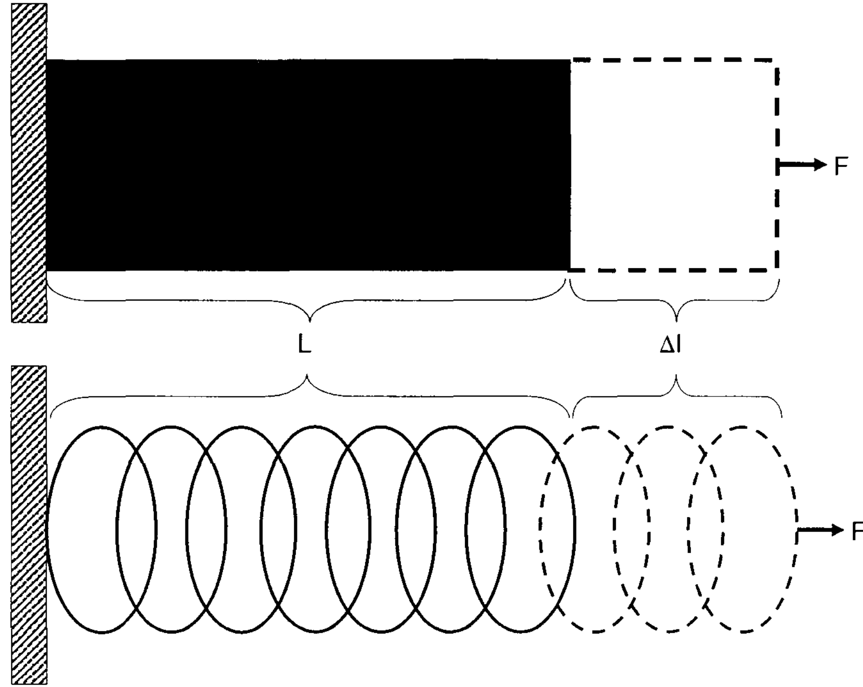

Figure 2·1: Beam and spring relation

as;

$$\delta L = \epsilon L = \frac{FL}{Ewt} \tag{2.3}$$

As we said before an elastic beam can be considered as a spring, Fig.2·1. So one can establish a relation between the applied force and the elongation, as a spring.

$$\begin{aligned} F &= k(\epsilon L) \\ F &= k(\frac{FL}{Ewt}) \qquad (2.4) \\ k &= \frac{E(wt)}{L} \qquad (2.5) \end{aligned}$$

This equality shows that the main characteristic of a beam is the spring

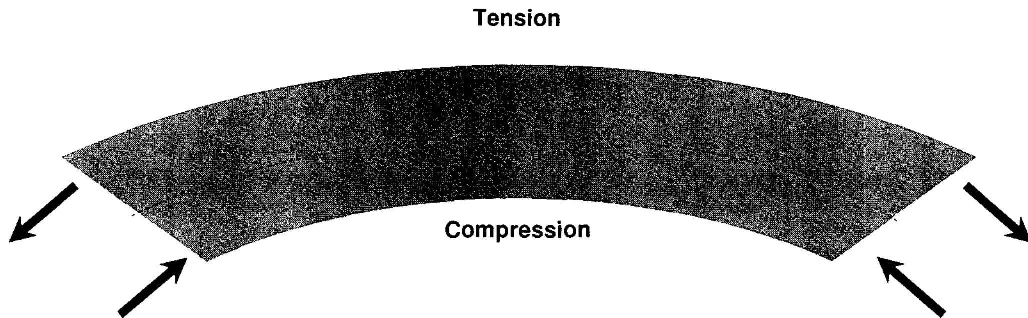

Figure 2·2: Tension and Compression Representation on a beam

constant (k). This entity covers both geometric parameters (w, t, ℓ) and material property (E).

This relation brings us the first design criteria for material selection. We should choose a material which has lowest possible Young's modulus, with consideration of other properties.

If the force is towards to the beam, this compressive force causes a buckling instead of expanding. So a curvature $(1/R)$ will occur. Under a compressive stress; upper half will expand and lower half will contract. Fig.2·2

Dotted line represents the neutral axis. Deformation occurs above and below this line. Now we'll examine the stress-strain relation on the beam. If the neutral axis is defined as:

$$dx = R d\theta \tag{2.6}$$

then elongation of the beam becomes;

$$dL = dx - zd\theta \tag{2.7}$$

and strain function in terms of z becomes

$$\epsilon = -\frac{z}{R} \tag{2.8}$$

Stress function in terms of z has the form of

$$\sigma = -\frac{zE}{R} \tag{2.9}$$

Internal bending moment M is the first moment of internal stress.

$$M = \int_{-H/2}^{H/2} wz\sigma \, dz M = -\left(\frac{1}{12}wt^3\right)\frac{E}{R} \tag{2.10}$$

This shows that the beam has compressive stress down side where it has tensile stress on the upper part. This behavior creates buckling. Depends on the orientation of the tension and compression fields, buckling will occur either upward or downwards.

2.1.2 Bar Buckling

In the case of clamped-clamped beam, compression will lead to a buckling.Direction of the buckling will be either lateral or vertical. Previous studies (Chiao and Lin, 2000) showed that if the width of a beam is larger than the thickness ($w > h$), beams tend to buckle out of plane. And in the opposite case ($w < h$), lateral bending occurs.

Buckling is determined by the least second moment of the cross section area of the bar. Assuming the beam has the structure to realize out-of-plane buckling, second requirement is having a certain axial loading to start buckling, called the

critical load(P_{cr}).

A differential equation will define the deflection. The eigenvalue of this equation will be critical load and the eigenvectors will be the deflected beam. Since this system operates like a spring, the beam will have a restoring force to turn back the original position. If an external load goes below the restoring force, the beam will cease buckling. If it goes above the restoring force then buckling will occur.

For the design perspective we have two more parameters:

1. Desired thickness to width ratio ($w > t$)

2. Enough force to initiate the beam

For the fabrication limitations, the beam width will be $6\mu m$. The desired buckling is out of plane so thickness will be chosen smaller than this value which will be $1\mu m$ in our case. By choosing these values, it is guaranteed that the beam will have a negative curvature.

Knowing that I is the moment of inertia, $I = \frac{bh^3}{12}$, a doubly pinned beam has a critical load (James M. Gere, 2009) as follows:

$$P_{cr} = \frac{\pi EI}{L^2} = \frac{\pi^2 Ebh^3}{12L^2} \tag{2.11}$$

In order to get this load, required temperature increase can be shown as follows (McCarthy et al., 2007):

$$\Delta T_{cr} = \frac{P_{cr}}{\Delta\alpha Ebh} = \frac{(\pi h)^2}{12\Delta\alpha L^2} \tag{2.12}$$

In the case that the axial load is larger than critical load, we can examine the curvature (Jones, 2006) for the beam according to the following equation;

$$\rho = \frac{1}{R} = \frac{\pm(y\prime\prime)}{[1 + (y\prime)^2]^{(3/2)}} \tag{2.13}$$

y denotes the deflection function. If y is equal to zero, the beam does not buckle. If y is not equal to zero but smaller than 1, then denominator can be neglected. Because the square of the slope, $(y\prime)^2$, will have a small value with respect to 1.

In our design, the deflection is expected around 3-5 degree which corresponds a value less than 0.1 then $(y\prime)^2$ will be negligibly small. So for small deflections, the deflection function can be represented as;

$$\rho = \frac{1}{R} \cong \pm(y\prime\prime) \tag{2.14}$$

The beam equation is established from the equilibrium of bending moment (M) and restoring moment. Restoring force and deflection amount creates an opposite moment, $M_{rs} = F_{rs}y$ where

$$M = EIy\prime\prime \tag{2.15}$$

and

$$EIy\prime\prime = -F_{rs}y \tag{2.16}$$

This forms the differential equation mentioned above; Eqn.2.17

$$y\prime\prime + \frac{F_{rs}}{EI}y = 0 \tag{2.17}$$

Now we have a second order differential equation. In the form of:

$$y\prime\prime + ky = 0 \tag{2.18}$$

We have two initial values for this equation;

1. $y(0) = 0$

2. $y(L) = 0$

Our beam is fixed at both ends and we will see no deflection at these points. Under these *initial value* conditions, two linearly independent solutions needs to be defined in order to solve this equation. One can define the following equation as a solution;

$$y = Asin(kx) + Bcos(kx) \tag{2.19}$$

By using initial values, given above, we can find A and B

$$y(0) = 0 \Rightarrow B = 0 \tag{2.20}$$

$$y(L) = 0 \Rightarrow \tag{2.21}$$

$$i.A = 0$$

$$ii.kL = 0$$

$$\tag{2.22}$$

A cannot be zero. Then kL must be zero. Since this is a trigonometric function. $kL = n\pi = 0$ condition satisfies the solution and after substitution of k with $\frac{n\pi}{L}$ solution is obtained as in Equation 2.23. That will be the form of the buckling for our device Fig. 2·3.

$$y = Asin(\frac{n\pi x}{L}) \tag{2.23}$$

Bending moment of the beam is also shown in Fig.2·4 according to the equation below:

$$M = EIy''$$

$$M = -\mathbf{C}(sin(n\pi x)) \tag{2.24}$$

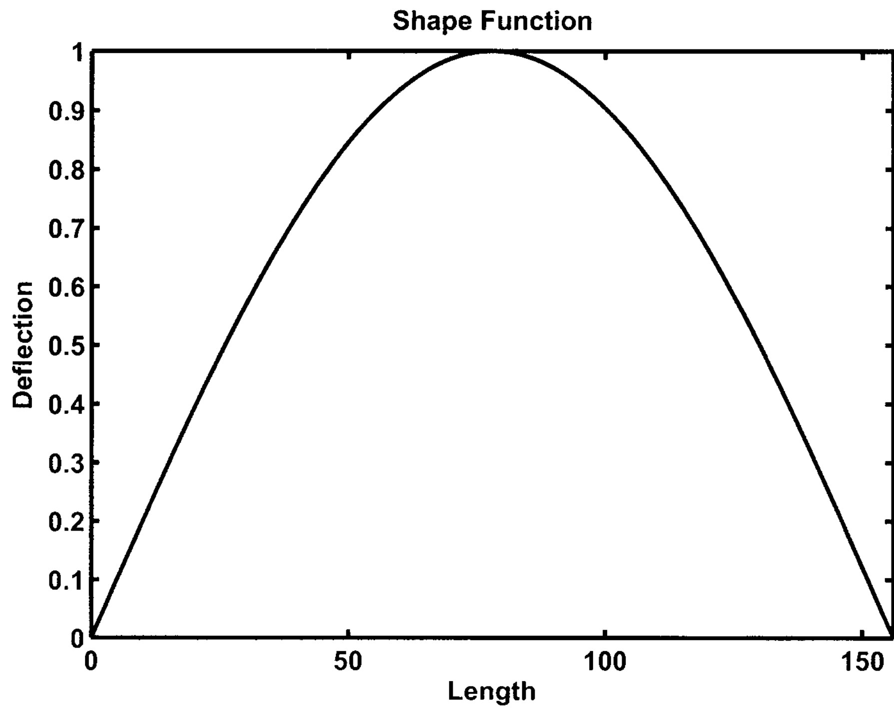

Figure 2·3: Shape Function of a doubly pinned beam

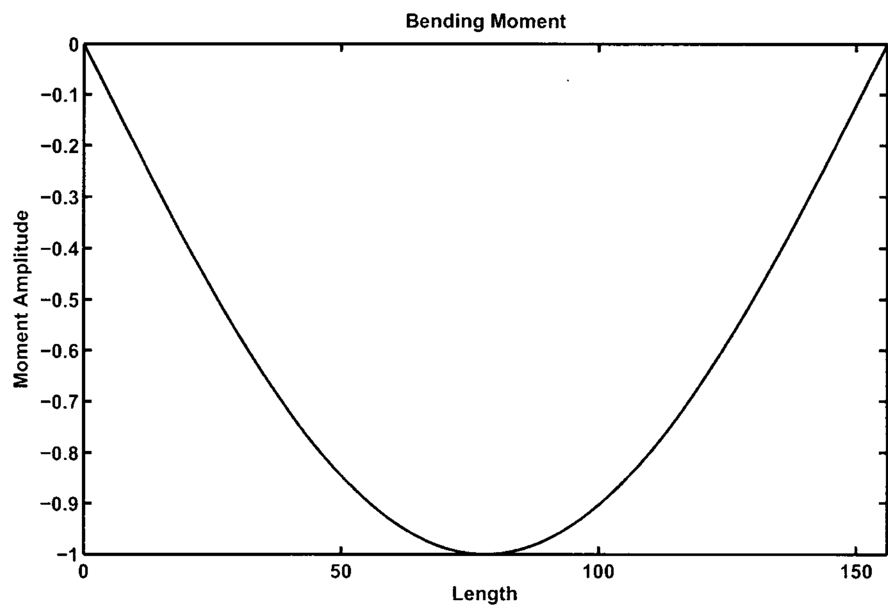

Figure 2·4: Bending moment of a doubly pinned beam

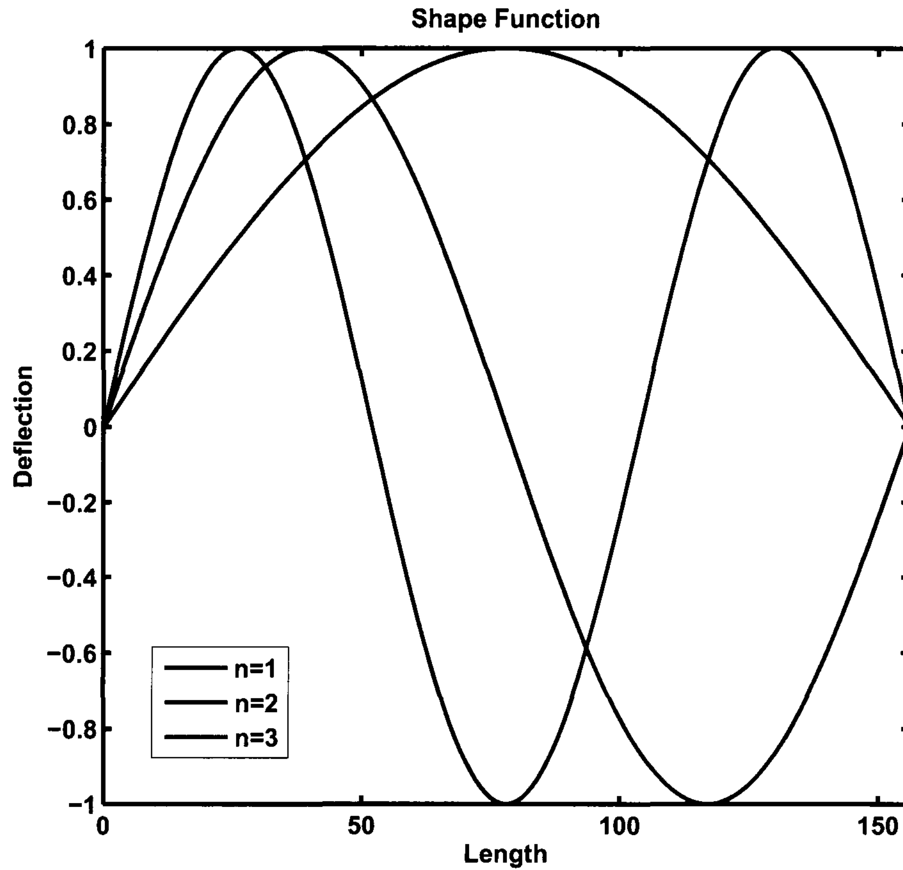

Figure 2·5: Shape Function of different modes

n is the number of modes. In order to realize 2nd and higher modes, some constraints need to be put on the beam and higher load need to be applied (Jones, 2006). There will be no constraints on the beam, we will only deal with first order mode. Different modes ($n = 1-3$) and their shape functions are shown in Fig.2·5

2.1.3 Heat Transfer Modal

Heat transfer for our structure will be investigated in three parts:

1. Heat Loss by conduction

2. Heat Loss by convection

3. Heat Loss by radiation

Now we will take a look these aspects one by one.

Conduction Heat loss with this type occurs between solids. As a definition; *"conduction may be viewed as the transfer of energy from the more energetic to less energetic particles of a substance due to interaction between particles"* (Incropera and De Witt, 1990)

In order the to quantify the energy transfer, we will use the rate equation per unit time. The rate equation for conduction is known as Fourier's Law where k is *thermal conductivity* and T is *temperature.*

$$q'' = -k\frac{dT}{dx} \tag{2.25}$$

This equation shows that heat flux will be in the direction of decreasing temperature. Since our device is negligibly short ($1cm$) we'll assume that the temperature is uniform through out the chip. Heat loss will occur between contact pads and substrate. In this respect 2.25 becomes;

$$q'' = k\frac{T_1 - T_2}{L} \tag{2.26}$$

Convection Heat transfer through convection occurs in different ways. We will focus on transfer between a fluid and a solid surface at different temperatures.And convection heat transfer may also be classified by the nature of the flowing fluid as natural and forced. In our case this will be natural flow of air. Heat flux is known as Newton's cooling law and defined as;

$$q'' = h(T_\infty - T_s) \tag{2.27}$$

where h is the heat transfer rate that includes all parameters effect heat transfer such as surface geometry, nature of the fluid flow, transport properties, T_∞ is the ambient temperature and T_s is the temperature for the structure. In this part we will use the standard values for convection heat transfer rate (Incropera and De Witt, 1990).

Radiation Thermal radiation is temperature emitted by a surface at a finite temperature which is determined by emissivity characteristic (ε) of the material. Although radiation might emanate from different surfaces, we will focus on the one from a solid surface. σ is the *Stefan-Boltzmann constant* ($\sigma = 5.67x10^{-8} W/m^2K^4$)

$$q'' = \varepsilon\sigma(T_s - T_{sur}) \tag{2.28}$$

In a real experiment, if the setup is not in vacuum, all of these heat transfer types are possible. Then, total heat loss will include conductive loss, q_{cond}, through pads, connected to the substrate (Si), convective loss, q_{conv}, from the structure into the air and the radiative loss, q_{rad}, is represented as follows;

$$q = q_{cond} + q_{conv} + q_{rad} \tag{2.29}$$

$$q = k_{Si}(whL)\frac{T_1 - T_2}{L} + h(T_\infty - T_s) + \varepsilon_{Cu}(whL)\sigma(T_s - T_\infty) \tag{2.30}$$

w, h, L stand for *width*, *thickness* and *length*, respectively.

2.1.4 Electrothermal Heating

Electrical analysis of the electrothermal actuator begins with defining resistivity of the beam. Despite seemingly simple operation, it is not easy to define resis-

tivity qualitatively especially over a wide range of temperatures. For the sake of simplicity will consider that the temperature is independent from temperature. In other words our calculations will include the values after the temperature reaches a steady state value. Now we can define the resistivity. This approximation is valid because the longest part that the current will flow is less than a centimeter so in this short length, temperature distribution can be considered as uniform.

$$\rho = \frac{VA}{J\ell} \tag{2.31}$$

V is the potential difference along the length ℓ, A is the cross-section of the beam and J is the total current through the beam. Energy generated by electricity is;

$$W = VI\Delta t \tag{2.32}$$

The energy, needed to increase the temperature (ΔT) of the beam is;

$$Q = cm\Delta T \tag{2.33}$$

The increase in temperature is given below:

$$\Delta T = \frac{VI\Delta t}{cm} \tag{2.34}$$

The equation above is valid when there is no heat loss. Heat loss will be included in the following section.

2.1.5 Finite Element Analysis of Mechanical Modal

Simulations has been done with a commercially available finite element analysis software, COMSOL[1].

---

[1]COMSOL Multiphysics 3.5a, COMSOL AB

Simulations include three main components:

- Conductive Media
- Heat Transfer
- Solid, Stress-Strain

Each module has certain boundary conditions (BC). Those BCs will be explained with an accompanying simulation result.

- Conductivity us given as $58.1 \times 10^6 [S/m]$. Charge distribution through out the material is found by the Ohm's Law

$$J = \sigma E + J^e \tag{2.35}$$

which states that the current density is depends on the material property(σ), applied E-Field and externally excited current density. Left electrodes have 2V potential, right electrodes are grounded. Rest of the structure is restricted with electric insulation, means that the current is defined by the geometry Fig.2·6.

- Heat transfer module includes conduction and convection heat transfer equations. Temperature value (T), outcome of the Conductivity module,will be an input for this module Fig.2·7.

- Solid, Stress-Strain module uses T value as an input for thermal expansion. Structure is fixed with electrodes to the substrate. Reference temperature is 300 ^{o}K and expansion temperature will be T, so temperature difference will be $T - 300$ and expansion coefficient for the structure will be $\alpha = 16.5 \mu m^{-1} K^{-1}$, Fig.2·8.

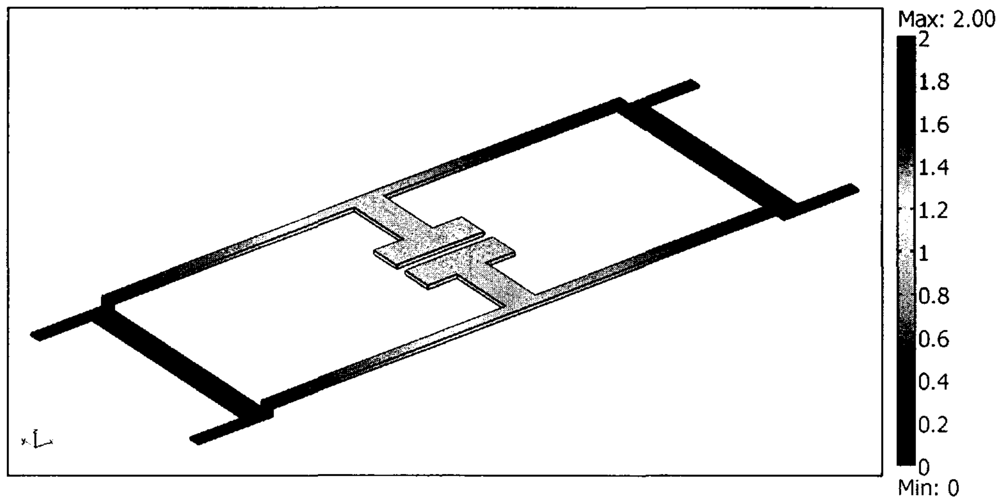

Figure 2·6: Voltage distribution on the structure

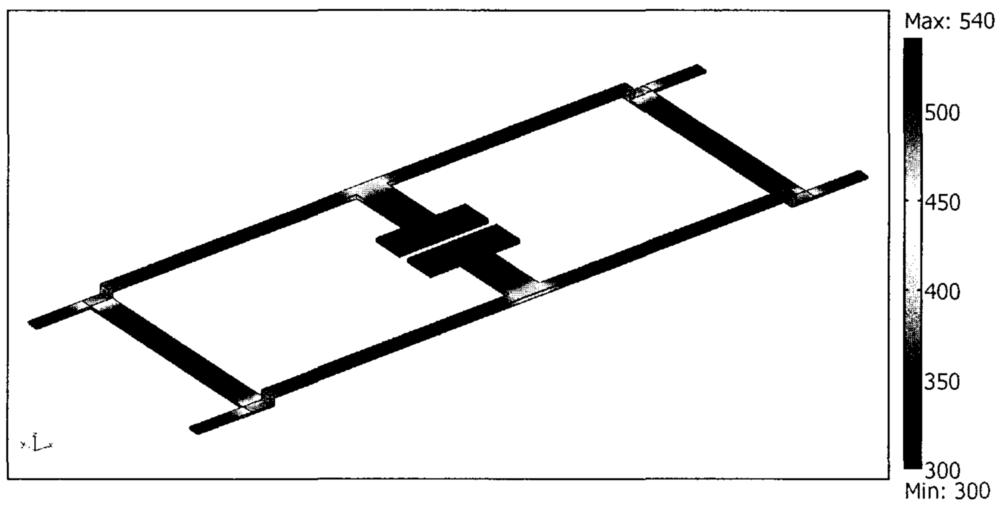

Figure 2·7: Temperature distribution of the device

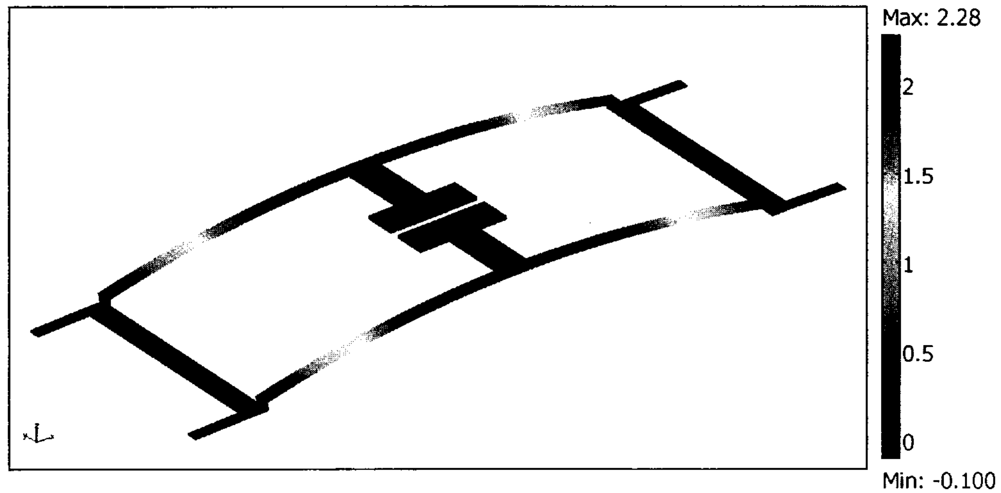

Figure 2·8: z-Displacement is shown for a thermal expansion

2.2 Electromagnetic Design

2.2.1 Effective Medium Theory

A material is called *homogeneous* when the refraction phenomena dominates over scattering/diffraction phenomena (Caloz and Itoh, 2006). Most of the naturally occurring materials satisfy this condition.

Once a material satisfies the homogeneity condition, it is called an *effective medium*. An effective medium is comprised of unit cells. The unit cell size (a) needs to be much less than wavelength (λ) of the incident light, ($a < \lambda$). *Caloz* et.al. called this criteria as *homogeneity limit* or *effective-homogeneity condition.* If a material satisfies this condition, an electromagnetic wave will see an average value of optical property instead of macroscopic device property. This kind of engineered material is called a *metamaterial.*

The novel optical properties, not found in natural materials, are distinguishing characteristics of metamaterials. Metamaterials has two main optical property, can be manipulated by design, electric permittivity (ε) and magnetic permeability (μ).

Negative permittivity and permeability proposed by a Russian physicist Veselago (Veselago, 1968) in 1967[2]

Permittivity

Permittivity describes the susceptibility of a material to an electric field. The higher the permittivity, the greater the polarization induced by an electric field.

A capacitor is a passive component that working principle is based on electric permittivity. As it can be seen at Figure 2·9 capacitor is comprised of two conductor plates with a dielectric medium in between.Parameters of these components determine the capacitance; d, distance between the conductor plates; overlapping area of these plates (A) and dielectric permittivity of the medium in between the plates.The relation between those parameters is shown in equation below;

$$C = \frac{\varepsilon}{A} d \tag{2.36}$$

The dielectric constant of a material is defined relative permittivity with respect to permittivity of air ($\varepsilon_0 = 8.8542 \times 10^{-12} F/m$) (Saleh and Teich, 2007).

$$\varepsilon = \varepsilon_r \varepsilon_0 \tag{2.37}$$

$$\frac{\varepsilon}{\varepsilon_0} = (1 + \chi) \tag{2.38}$$

χ is called *electric susceptibility.*

Permittivity value has also effect on polarization density $\mathbf{P}$ of the material with the following relation;

[2] In the English translation, publish year indicated as 1964 by mistake(Marques et al., 2006)

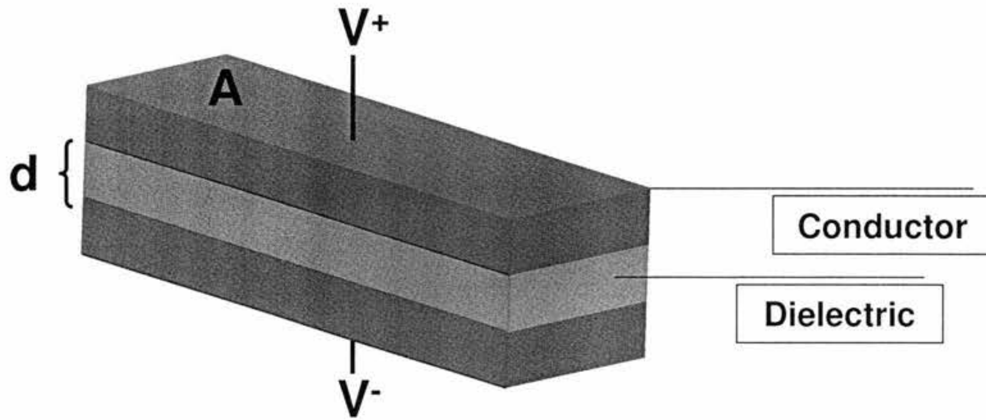

Figure 2·9: Capacitor

$$P = \varepsilon_0 \chi E \tag{2.39}$$

Similar conditions apply for the *magnetic permeability*, μ. It builds the relation between *magnetic flux density* and *magnetic field*;

$$B = \mu H \tag{2.40}$$

Same as dielectric constant, permeability may be defined relative to the vacuum permeability $\mu_0 = 1.2566 \times 10^{-6} H/m$.

$$\mu = \mu_r \mu_0 \tag{2.41}$$

$$\mu = (1 + \chi_m)\mu_0 \tag{2.42}$$

where χ_m is called magnetic susceptibility.

2.2.2 Split Ring Resonators

Split ring resonators are well studied structures for Microwave range devices. In 1999 (Pendry et al., 1999), this structure introduced into metamaterials area. More recently, SRRs have been investigated at higher frequencies including THz. In this study will focus on resonance characteristic of our device and how it changes with external electric stimuli.

Resonance Frequency

A resonator shows a resonance characteristic at certain frequency more than other frequencies. Both electrical and optical resonators have same behavior. They oscillate larger at a certain frequency. If an input signal has the same resonance, it is absorbed by the resonator or if it is a wide band signal, resonance band selected/absorbed by the resonator. This frequency is called *resonance frequency* and it is denoted by w_0.

If we think an electric circuit, comprised of passive elements; such as R, L, C. In resonance, reactance of both capacitor and inductor are equal.(Eqn.2.43)

$$R_C = \frac{1}{wC} \tag{2.43}$$

$$R_L = wL \tag{2.44}$$

Then the resonance frequency will be at the point of which reactance of the capacitor (R_C) and the reactance of the inductor (R_L) are equal to each other. In other words; at that point, both maximum magnetic energy and maximum electrical energy is equal to each other (Konishi, 1998). A related LC circuit is depicted in Figure 2-10

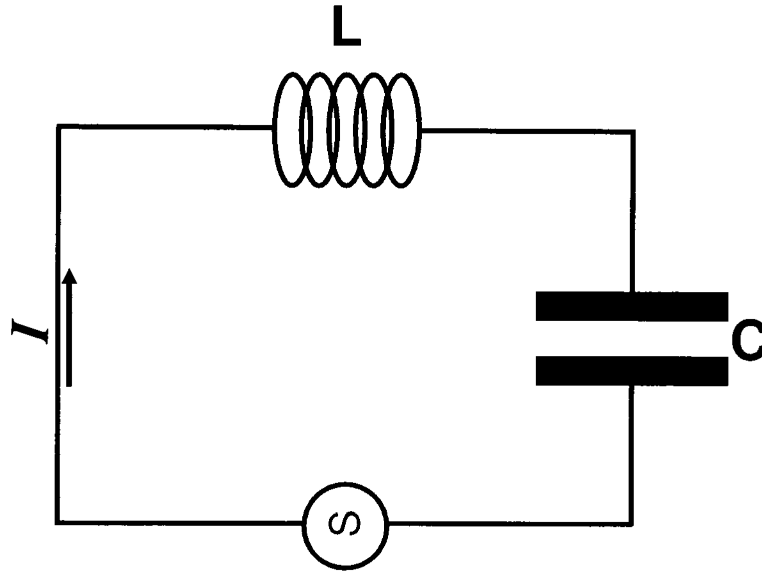

Figure 2·10: Circuit schematic of a capacitor (C) series in an inductor (L)

$$wL = \frac{1}{wC} \tag{2.45}$$

$$w = \frac{1}{\sqrt{LC}} \tag{2.46}$$

Electric Circuit Modal of Split Ring Resonators

It has been shown that this structure is able to show either electrical or magnetic or both responses, depending on the configuration of the incident wave.(Katsarakis et al., 2005)

In this study we will be dealing with electric resonance characteristic of SRR. Since the configuration defines the response characteristic, the device will be polarization sensitive.

The basic SRR structure is shown figure below. And its electric circuit equivalence is also shown in adjacent figure. A simple SRR structure and its equivalent

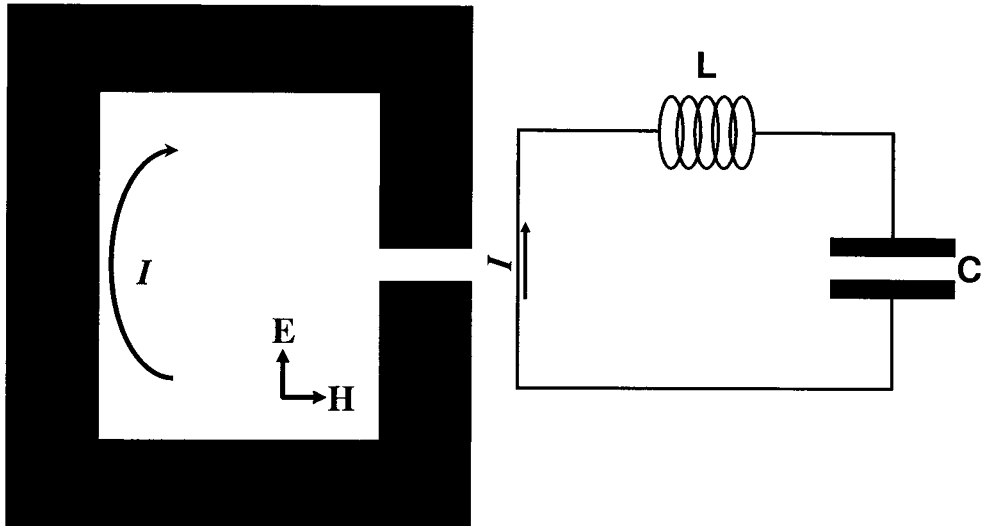

Figure 2·11: SRR structure and its electrical circuit equivalence

electric circuit is shown in Figure 2·11

So the resonance frequency becomes;

$$w_0 = \frac{1}{\sqrt{LC}} \tag{2.47}$$

Baena et.al.(Baena et al., 2005) investigated electromagnetic responses of SRR structure in different wave configuration. This study shows that SRRs can be excited magnetically and/or electrically if the structures is aligned in a correct orientation. Our design will have an electric resonance and field configuration according to that purpose.

Mirrored Split Ring Resonator (mSRR) and Equivalent Electric Circuit

We will focus on electric resonance of the SRR structure. For this propose we picked the mirrored SRR. This structure comprised of two adjacent SRR which are mirrored vertically. This structure will cancel any possible magnetic excitation because of its symmetry 2·12. Because electrically induced circulating

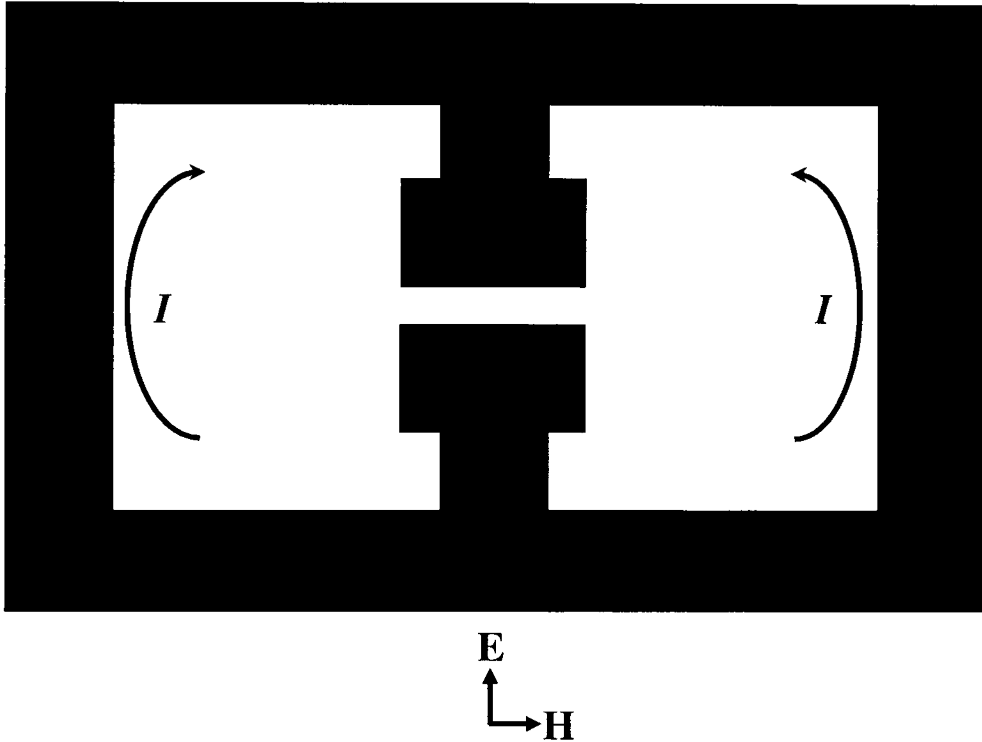

Figure 2·12: Mirrored Split Ring Resonator field configuration

current will create a magnetic field. As shown in Figure 2·13 circulating currents have opposite directions. Magnetic fields, created by circulating currents also have opposite directions, so magnetic fields always will be canceled out. That will give us pure electric response of the device. This is possible with the depicted (Fig.2·12) configuration of the fields.

In Fig.2·13 equivalent circuit schematic of the mirrored SRR is shown. Regarding this circuit, resonance frequency of this LC circuit will be:

$$w_0 = \sqrt{\frac{2}{LC}} \tag{2.48}$$

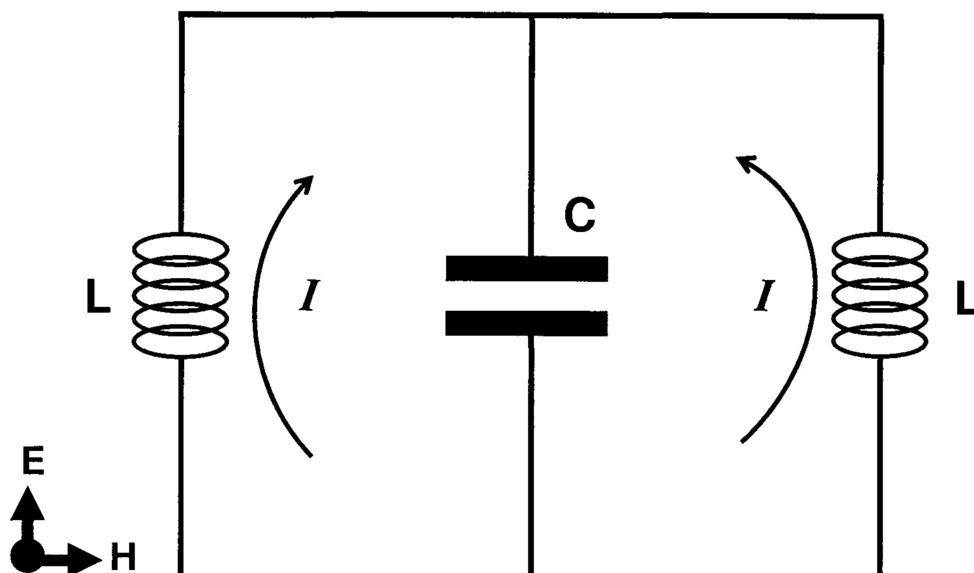

Figure 2·13: Equivalent circuit of mirrored SRR structure has two parallel inductors and one capacitor is shunted to them.

Active THz Metamaterials

As mentioned before, metamaterials display a novel behavior, unique from natural materials. The main idea behind making active metamaterials is to tune or change the properties in response to some external stimulus. This could be done either by changing capacitance or inductance. This idea had been realized by different groups (Chen et al., 2006),(Padilla et al., 2006), (Paul et al., 2009) using different methods. In the present thesis, this is accomplished by using resistive heating to induce motion of the SRR. This motion will change the capacitance of the device.

At first, previous studies will be explained briefly in the following section.

In 2006, Padilla et. al had the result of shifting transmission resonance frequency by photo-excitation of free carriers in GaAs substrate (Padilla et al., 2006). Since photo-excitation of carriers shorts out the capacitor gap and this effect turns-off the electrical resonance.

In the same year, Chen et.al demonstrated a tunable THz metamaterial (Chen et al., 2006). The device is comprised of oppositely combined split ring resonator (SRR). The device has been designed in a way that worked as a Schottky diode. An increasing gate bias voltage (0-16 V) enlarge the depletion region, thus decreasing the conductivity of gap and increasing capacitance, changes the resonance frequency.

In 2009 Paul et.al proposed a polarization independent active metamaterial (Paul et al., 2009). They have used the same principle which Chen et.al demonstrated in (Chen et al., 2006). However there are two significant improvements in this work. First the device is insensitive to polarization of incident wave. Secondly they claim that this design can realize amplitude modulation up to 100 KHz.

Three of these studies used either photo-excitation or electric excitation in order to realize a frequency shift. In our project we proposed a different approach to this problem. Our device will provide frequency shift by electro thermal actuation.

In this study, we aim to produce a new device that have the functionality of an active THz metamaterial in a different method. We utilize a metamaterial as an actuator. While mSRR is actuating mechanically, its optical property will change. Detailed working principles is in the following section.

Working Principle of the ETAMM

Electrothermally actuated THz Metamaterial ($ETAMM$) will be investigated in two in two interrelated parts; one, mechanical actuator and second, an electromagnetic (EM) resonance. Tuning an electromagnetic resonance is the outcome of this combination.

Mechanical actuation initiated by conducting electricity through the electrodes on the substrate. They will carry the current to the device. Current will

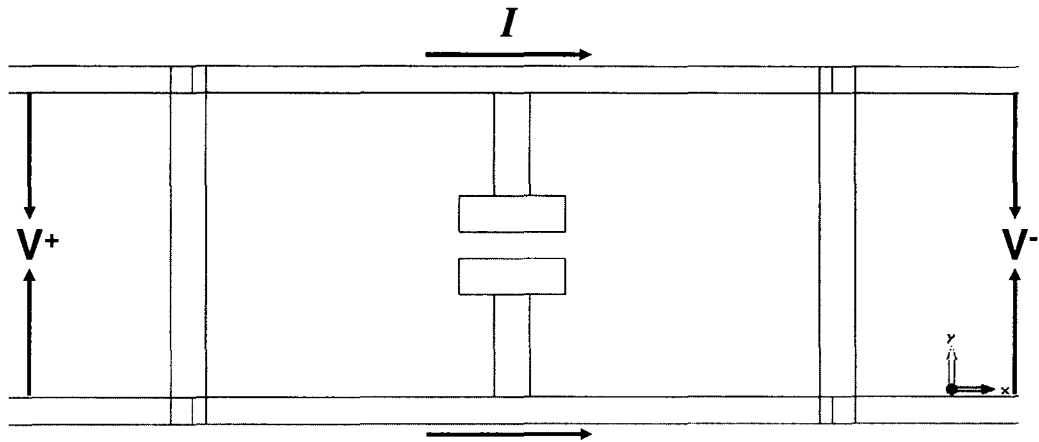

Figure 2·14: Due to a potential difference between two ends of the device, there is a current flow. This current flow causes a resistive heating

cause a resistive heating on the suspending legs (Fig.2·14). Straight legs will bend up and this bending will change the distance between the legs and the dielectric substrate. Thus this change results as altering in the capacitance. Since capacitance is created by electric field line between two conductors, separated by a dielectric, any change on the electric field lines will reflect on the capacitance (Fig.2·15).

As mentioned before resonance frequency in LC circuits is depends on capacitance and inductance. By manipulating capacitance of the circuit, one can tune the resonance frequency. Tuning with capacitance is chosen for this project because inductance change requires big change on geometry like large elongation, or increasing thickness at least double fold. On the other hand capacitance change can be obtained by small deflections. For instance if the distance between the plates is doubled, capacitance will be halved.

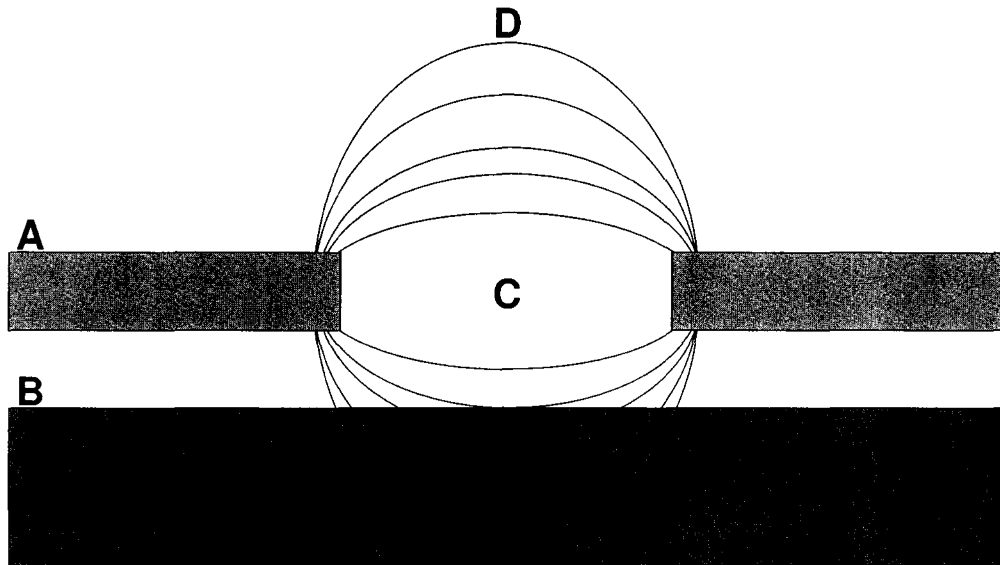

Figure 2·15: A capacitor modal with E-Field lines between conductor plates. Field lines passing through both air and substrate

Finite Element Analysis of Electromagnetic Modal

Simulations has been run on a conventional simulation software, CST[3]. Boundary conditions is set for field configurations, ambient property and library of the software is used for material property.

In order to get a electric LC resonance field configuration needs to be in a certain direction (Schurig et al., 2006). Linearly polarized EM field will have E-Field is on y axis, H-Field is on x axis and wave propagates into the plane (Fig.2·16)

This configuration creates a circulating current and E-Field concentrated on the gap. Figure2·17 shows that if the E-Field is not perpendicular to the gap, device will not exhibit a resonant response.

The new active THz metamaterial provides a resonance shift by electromechanical methods. Sweeping a frequency range by a precisely controlled actuation

[3]CST Studio Suite 2009, CST AG

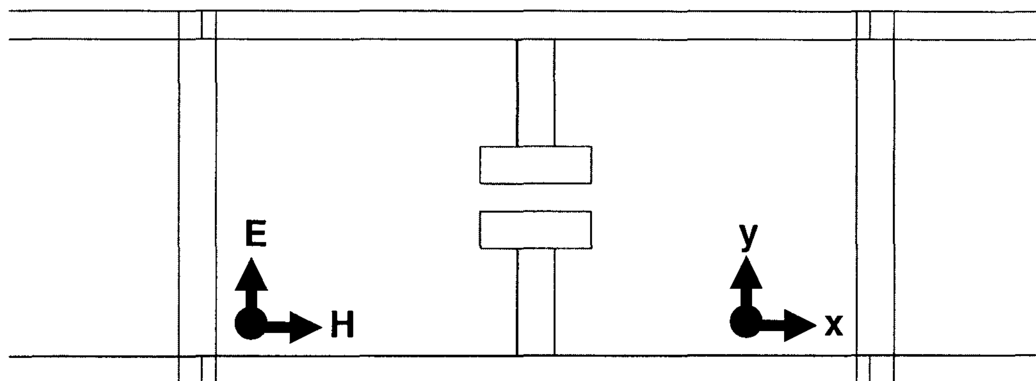

Figure 2·16: E-Field is on x-axis, H-Field is on y-axis, the wave propagates into the plane

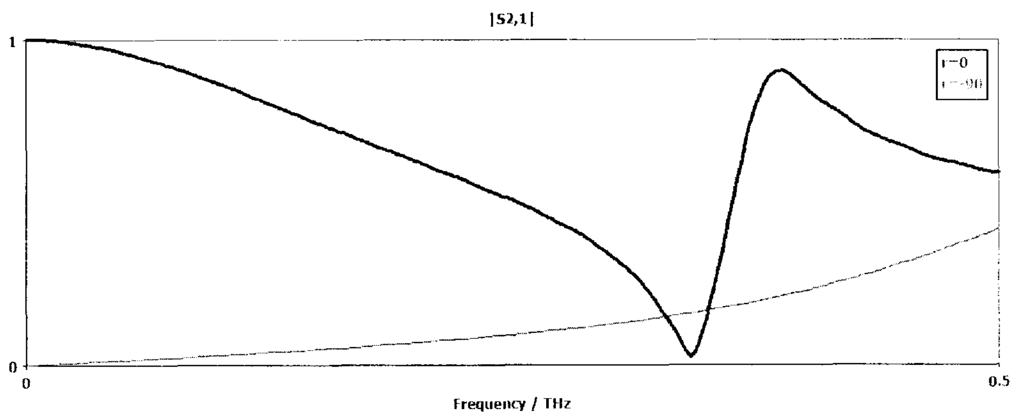

Figure 2·17: Thick line (red in online copy) is the transmission data of mSRR with no rotation, thin line (gray in the online copy) is the transmission data with the device has 90 degree clockwise rotation

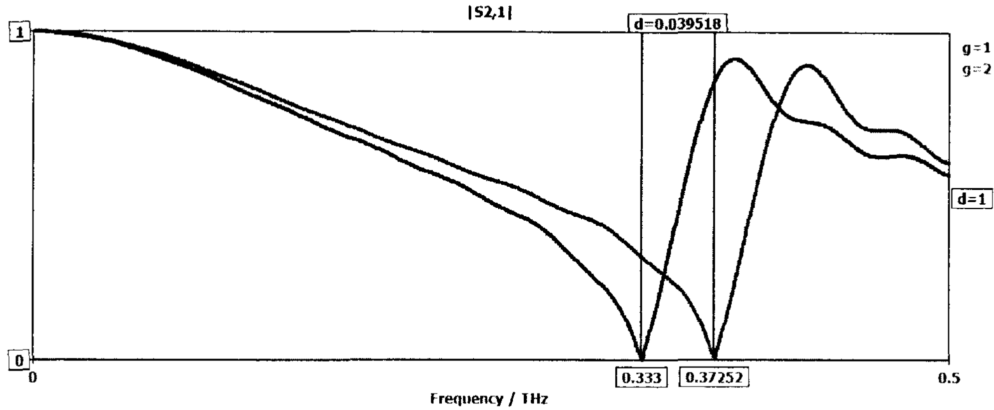

Figure 2·18: Red line (left curve) indicates the transmission when g=1, green line (right curve) indicates transmission when g=2. This simulation result shows nearly 40 GHz resonance shift for 1micron deflection. Height of the device is 1 micron over the substrate before deflection. g is the gap distance between the structure and the substrate

is the novelty of this this device. Frequency shift is not as large as previous study results. However by improving the device quality and experiment environment, larger frequency shift is possible.

Simulation results are depicted in Fig.2·18 and Fig.2·19. Fig.2·18 transmission data is for the proposed structure. Deflection amount is the value, obtained from mechanical simulations. The device has a 1 μm gap distance (g) between the structure and the substrate. After electrothermal heating, it deflects 1 μm over the substrate. This deflection delivers a resonance shift around 40 GHz.

In Figure2·19, deflection amount is the real value, obtained from the interferometric measurements. In this case initial gap distance (g) is 2.1 μm and the deflection amount is 0.8 μm. Under these conditions, frequency shift is delivered as around 15 GHz.

Optimization for the Device Geometry

The device geometry has some parameters such as length of the beam, width of the beam, thickness of the beam. In order to get the best output from the device

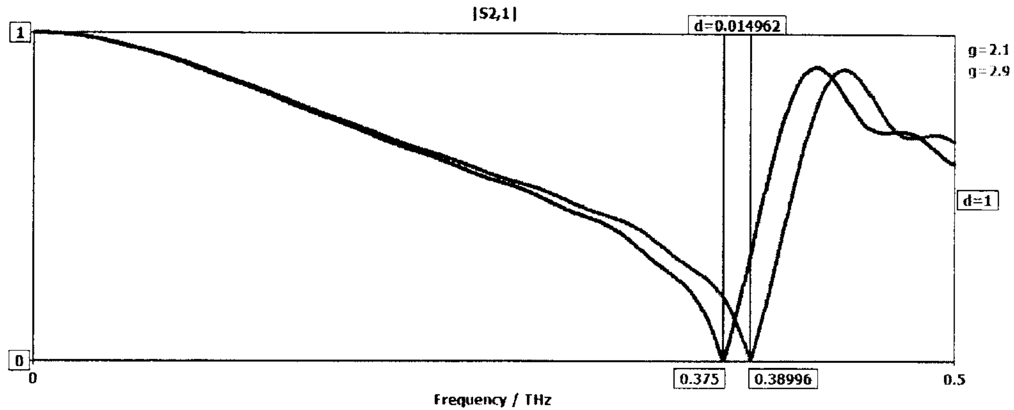

Figure 2·19: Red line (left curve) indicates the transmission when g=2.1, green line (right curve) indicates transmission when g=2.9. This simulation shows about 15 GHz resonance shift for 0.8 micron. Height of the device is 1 micron over the substrate before deflection (g is the gap distance between the structure and the substrate)

some optimization simulations are done on the structure.

First, we examine the effect of the beam length on the resonance shift. Simulations showed that the larger the beam length, the larger the frequency shift. Having the effective medium condition, there is a constraint on the beam length so having a beam length around $150\mu m$ is a correct choice. Figure2·20, Figure2·21, Figure2·22 shows resonance shift for beam lengths of 50, 100 and 150 respectively. It can be clearly seen that resonance shift increase is in direct relation with length increase.

We also run the simulation for different capacitor plate length and different width of the suspending beam and it is shown that there is not a significant contribution to resonance shift.

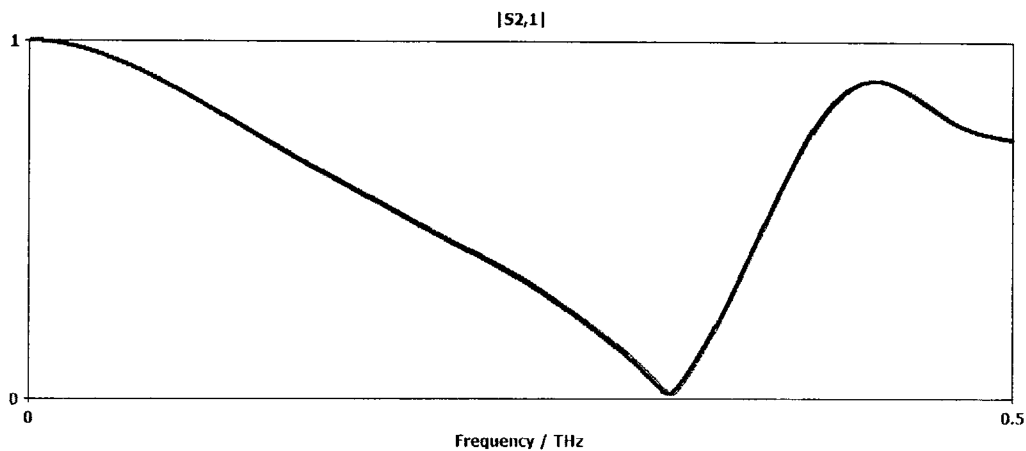

Figure 2·20: Resonance shift for a beam length of 50 μm. E-Field is on x-axis, H-Field is on y-axis, the wave propagates into the plane

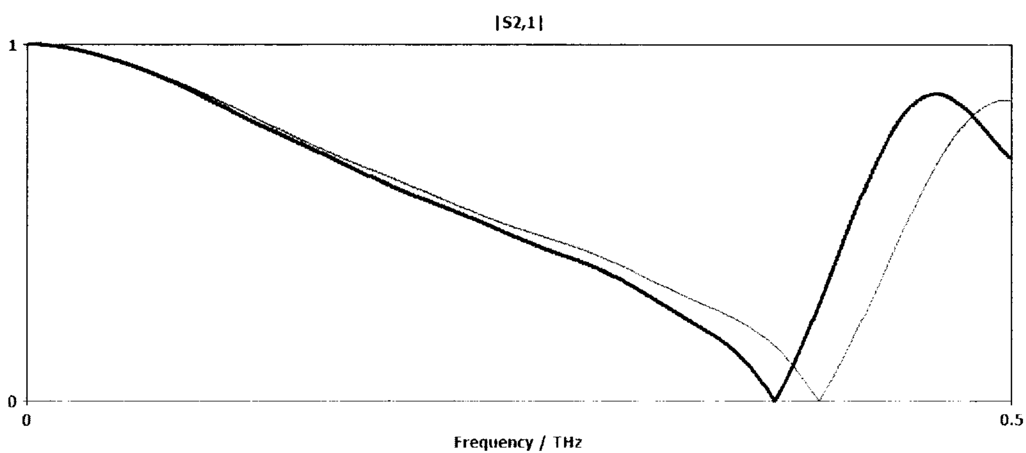

Figure 2·21: Resonance shift for a beam length of 100 μm. E-Field is on x-axis, H-Field is on y-axis, the wave propagates into the plane

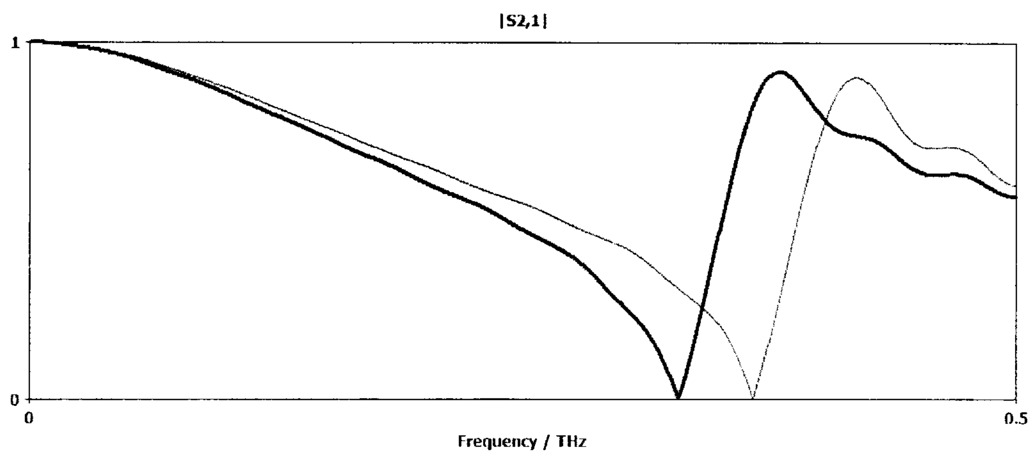

Figure 2·22: Resonance shift for a beam length of 150 μm. E-Field is on x-axis, H-Field is on y-axis, the wave propagates into the plane

Chapter 3

Fabrication

3.1 Fabrication Steps

The fabrication process is comprised of five steps, including three photolithography. In other words three consecutive layers are performed, with three different masks, on a 2 inch wafer.

The first step starts with *spin coating* of S1813 [1] Shipley photoresist at 4000 *rpm* for 45 seconds. Spin coating starts with spreading part at 500 *rpm* for 5 second and increases to 1000 *rpm* in 5 seconds. After spreading photoresist, spinner accelerates to 4000 *rpm*. Prior to this process as an adhesion promoter hexamethyldisilazane[2] (HMDS) is applied with same spinning recipe. Spin coating is followed by a *soft baking* at 90 $°C$ for 1 minute on an hot plate. Soft baking intends to evaporate the solvent in the photoresist; after this step photoresist becomes ready for UV exposure.

Exposure is performed by optical lithography machine [3]. For S1813 Shipley photoresist, *hard contact* type chunk position is choosen. This position of the chunk help to decrease scattering UV light before it reaches to photoresist. Exposure energy is set for $80mJ/cm^2$ (10 mW × 8 seconds). After exposure, wafer is immersed into MF 319 resist developer [4] for 45 seconds, in order to remove the exposed areas and reveal the pattern.

[1]Microposit S1800 Series Photo Resist. Shipley Company, Marlborough, MA USA
[2]Product No.00692. Polyscience, Inc. 400 Valley Road, Warrington, PA 18976 USA
[3]MJB3 Mask Aligner, Karl Suss MicroTec AG.
[4]Microposit MF-319 Developer. Shipley Company, Marlborough, MA USA

Figure 3·1: Ti/Au is deposited as seed layer with E-Beam Evaporation

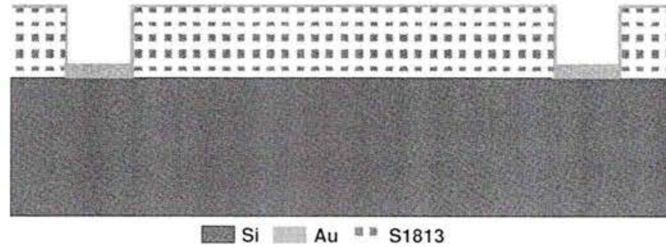

Figure 3·2: Sacrificial layer is coated and Second Au layer is deposited

After we had the pattern, Ti/Au 10/200 nm, seed layer is deposited with E-Beam evaporation[5] in low pressure, 5×10^{-6} mTorr. After metal deposition lift off process is applied sonication while the wafer in Acetone for 5 minutes. This sonication is applied for Isopropanol and water for same amount of time, in order to clean all metallic residue caused by lift off. Figure Fig.3·1 shows the wafer at the end of the first step.

The second step includes similar recipes. S1813 applied, after HMDS coating. Same power settings is applied for Mask Aligner. This layer will be built on top of the first layer, so alignment of these layers is essential. After photolithographic process is completed, Au (100 nm) is deposited with E-Beam evaporation. There is no lift-off process. Because this photoresist layer serves as a sacrificial layer.Figure 3·2

The third step starts with spin coating of S1818[6] photoresist. Spinning duration is reduced to 30 seconds, in order to get thicker (around 2 μm) coating.

[5]Electron Beam Evaporator BOC Edwards Auto 306

[6]Microposit S1800 Series Photo Resist. Shipley Company, Marlborough, MA USA

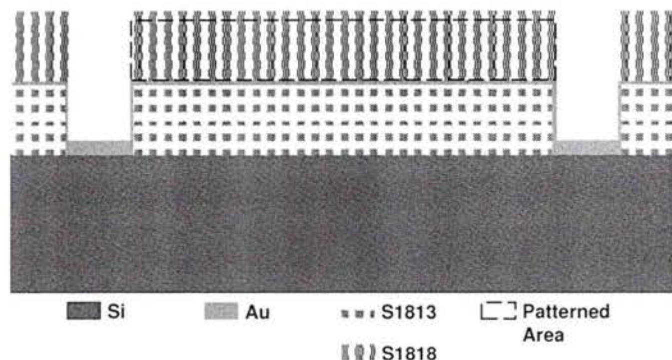

Figure 3·3: S1818 photoresist is coated and patterned. Cu is electroplating for the main structure

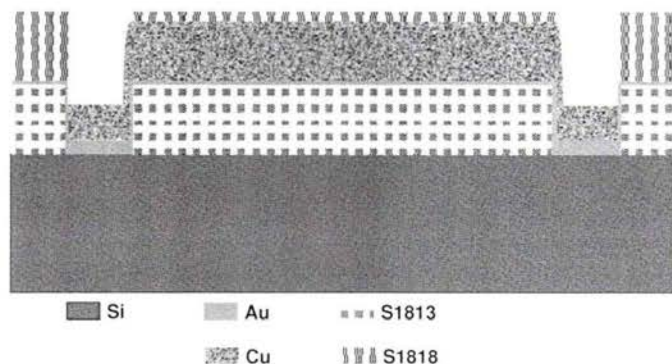

Figure 3·4: The last Au is deposited on the electroplated Cu structure

Mask Aligner is set to 10 seconds at $10mJ/cm^2$ dosage. Same as the second layer, aligning the marks precisely is crucial at this stage. After exposure, photoresist is dipped in MF-319 developer for 1 minute. Electroplating Cu on the patterned photoresist follows this process. Cu is electroplated in Copper Sulfate (Cu_2SO_4) solution with 47mA current. Figure 3·3 shows before and after electroplating.

In the forth step, the last Au layer ($100nm$) is deposited on Cu structure. After three consecutive fabrication steps, the device is ready for dicing and release process. Dicing saw [7] is used at 2000 rpm to have individual chips from 2" wafer.

The fifth step includes two parts. One is removing the sacrificial photoresist

[7]Type:CA-003-1800-030-H, Dicing Blade Technology

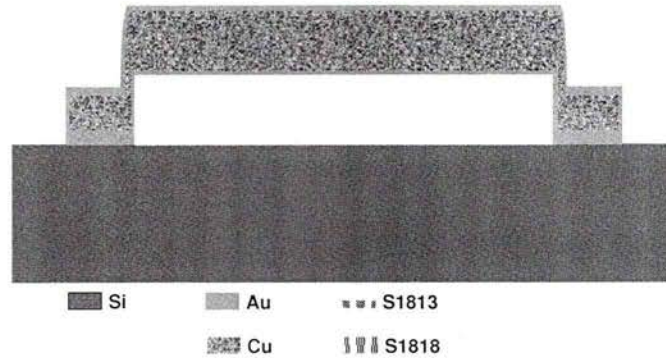

Figure 3·5: Released structure after CPD process

and releasing the structure with Critical Point Dryer. Photoresist removal is performed by dipping the chips into Acetone and keeping in the sonication device for 15 seconds at first. And solution is renewed and sonication is applied 15 seconds more. This process is repeated until all the excessive Au particles are removed from the array. This process is observed by a conventional laboratory microscope while the sample is still in Acetone.

After removing photoresist, the last step is putting the device in a *Critical Point Dryer(CPD)*. This step is crucial for the device. Because after this step, the device will be able to work in a room environment. Released structures is shown in Figure 3·5. A Scanning Electron Microscopy (SEM) image of the suspending beam is shown in Fig.3·6. Operation process of CPD is explained in the following section.

Figure 3·7 has a top view of the ETAMM and Figure3·8 shows a whole array of mSRR structures. Width of the structure is $60 \mu m$ and the length is $160 \mu m$. This is slightly larger than our designed values. This difference might be because of the photolithography or electroplating. During the photolithography there is always a wedge instead of a perpendicular edge. Due to this slope, during electroplating process this cause an enlargement of the beam.

In the following figures, released arrays is shown. Figure3·9 is an image of

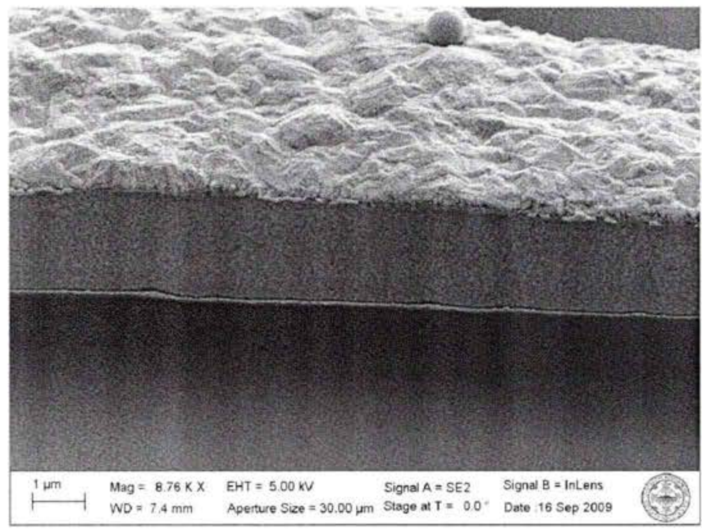

Figure 3·6: Suspending beam is about 1 micron above the substrate

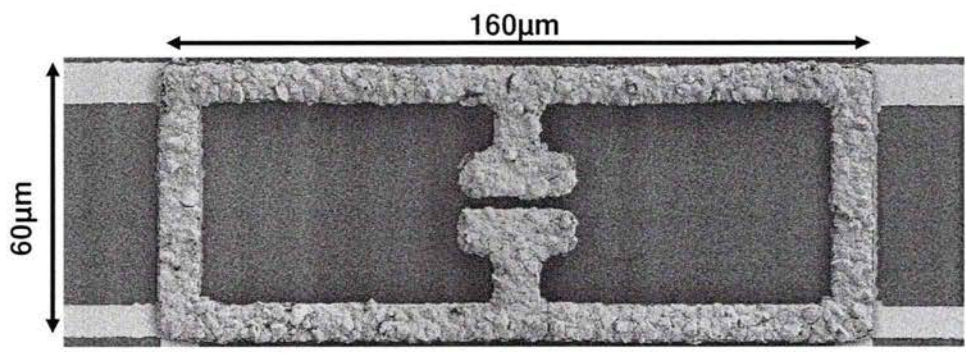

Figure 3·7: Top view of the released structure

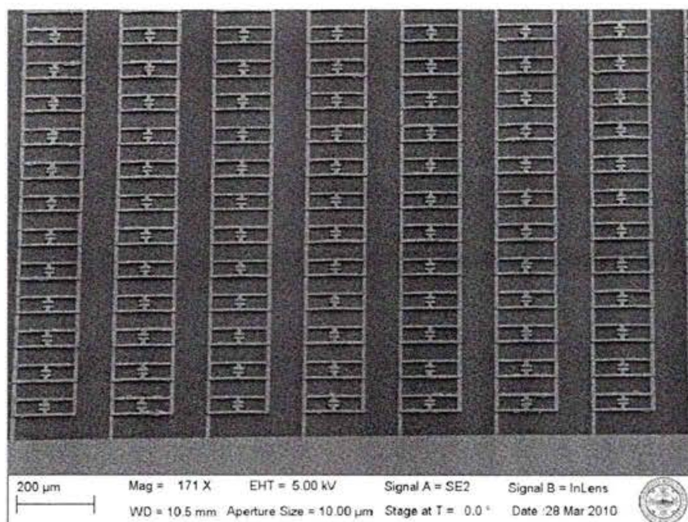

Figure 3·8: Scanning Electron Microscopy image of a suspending array

the array after sonication. This shows that structure is not robust enough to survive in sonication. The main reason of that is connection between seed layer and structure is not strong enough. In the following figure (Fig.3·10, a successful array is shown. In the image, array is in acetone and suspending.

Critical Point Dryer

CPD is a conventional method for having free standing structures. The working principle is based on critical evaporation point of liquid carbondioxide ($CO_{2_{liq}}$). In the Fig.3·11, essential parts of the Critical Point Dryer is shown.

First of all, released sample needs to kept in acetone to prevent stiction. Sample is transferred into a holder, filled with acetone. This holder is placed in the chamber and chamber door is closed tight. Then, $CO_{2_{liq}}$ is inserted into the chamber. Acetone is replaced by $CO_{2_{liq}}$. By increasing the temperature with a circulating heated water around the chamber, pressure is increased. As soon as pressure reached 1200 psi and temperature 35^oC, $CO_{2_{liq}}$ turn into gas phase. After $CO_{2_{liq}}$ is totally turned into gas phase, high pressure chamber is brought

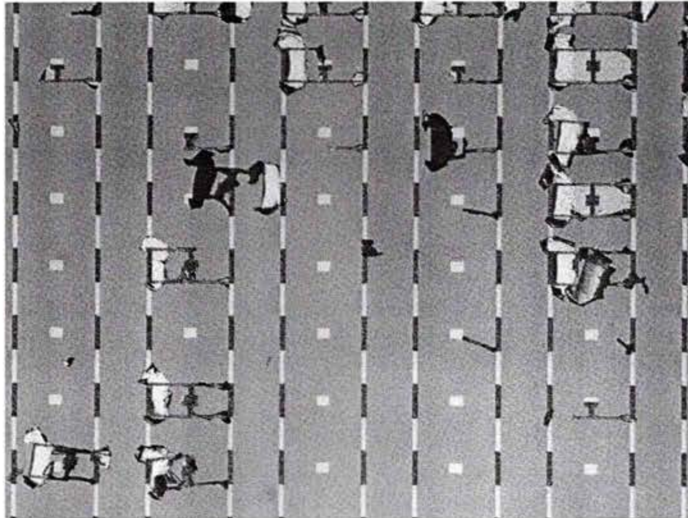

Figure 3·9: Damaged structure after sonication

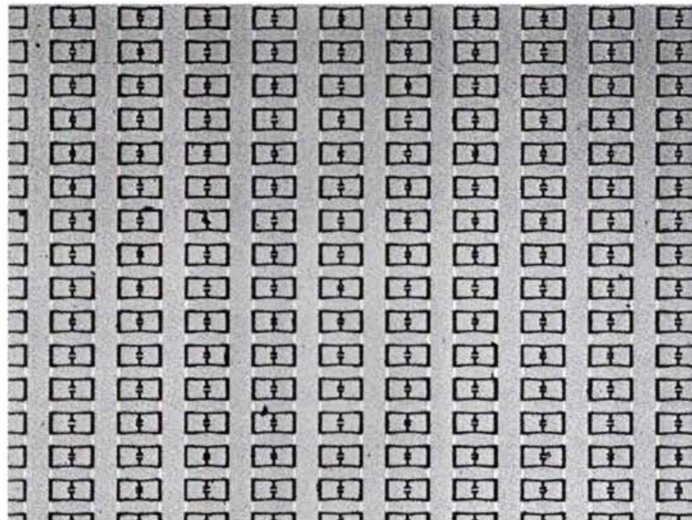

Figure 3·10: Suspending array after sonication

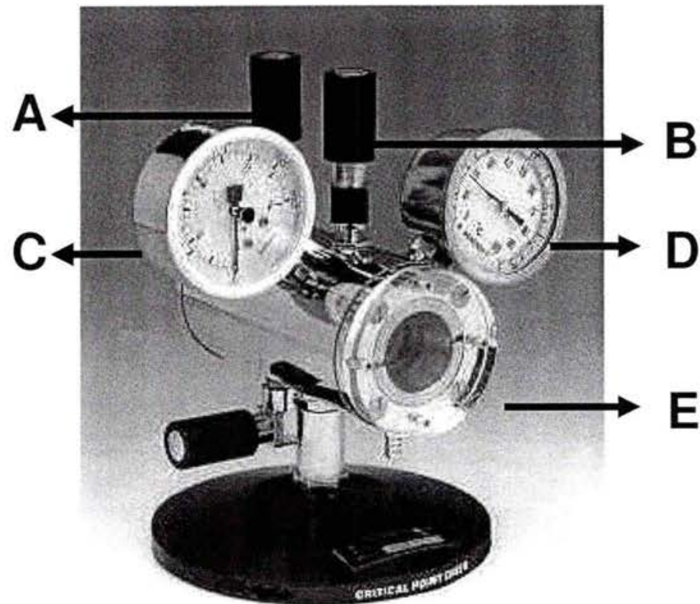

Figure 3·11: A:CO_2 liquid inlet valve, B:Air outlet, B:Pressure Display, C: Temperature Display, D: High pressure chamber, also heated up by circulating hot water within the cylinder

down to the atmospheric pressure. After this process, suspending structure can operate in room environment safely.

Chapter 4

Measurement

Interferometry provides a non-destructive and non-contact approach surface profiling of MEMS device. Interferometric profilometry has been used for thermal and electrothermal testing thereby providing information on thermal and distance change over a substrate.

4.1 Electrothermal

A DC power supply is connected to the device. The voltage across the device is increased gradually, from 0 V to 5 V, 1 V at a time.

4.1.1 Measurement Results

The following figures shows the electrothermal actuation of ETAMM. The measurement use a VEECO interferometer. In the first figure Fig.4·1 two axis show x and y projections. The x axis shows the curvature of the beam at post-release situation. The y axis shows the thickness of the structure.

In Fig.(4·2-4·6) x axis is shown highlighting the correlation between voltage and curvature is depicted. At 5V, deflection outcome is around 0.8 μm. This value is below the simulated value. There might be a couple of reasons. First is the oxidation of the copper. Even though it is covered by Au layer around.

Our first assumption is about the air exposure between electroplating and 3rd Au E-Beam deposition. Second assumption is about increasing temperature activity of Copper during thermal test. The temperature increase and dislocation

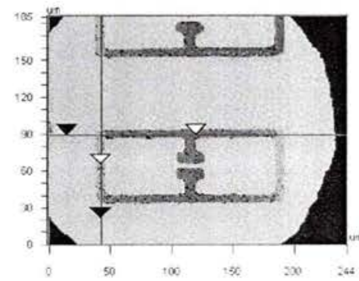

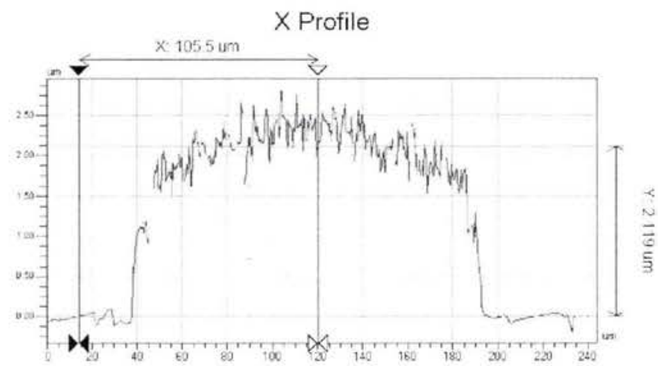

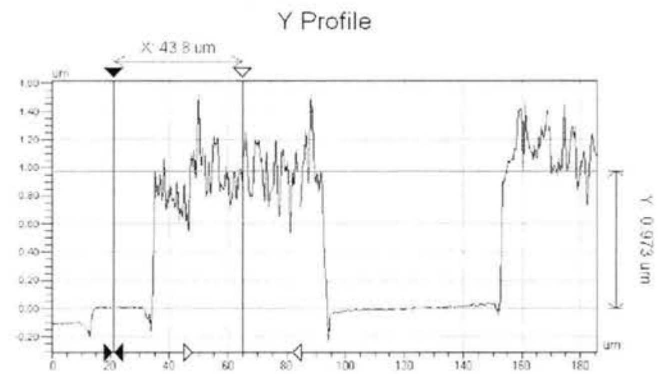

Figure 4·1: 2D profile, x and y axis projections of the structure at 0V applied

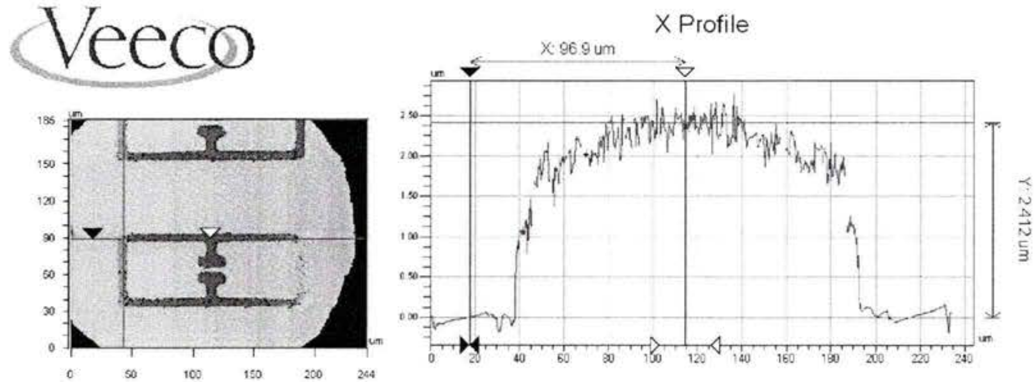

Figure 4·2: 2D profile, x axis projection of the structure at 1V applied

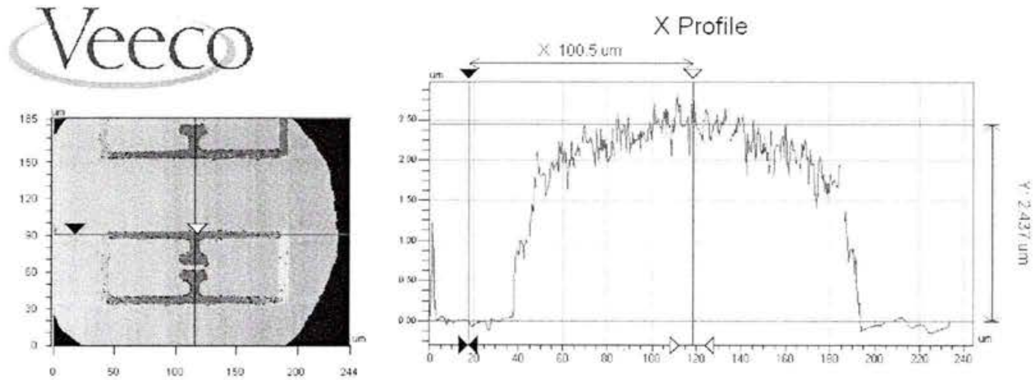

Figure 4·3: 2D profile, x axis projection of the structure at 2V applied

on the Au layer let the oxygen in. Another important reason might be unexpected heat loss. Convection heat transfer coefficient is an empirical value that depends on a number of parameters such as geometry, material properties, temperature etc. These are the parameters we can approximate and take them as constants during simulations. This difference between real values and library values cause different outcomes.

These uncertainties from the nature of the fabrication imperfections and parameter mismatch between real and library values lead to less deflection values than we simulated.

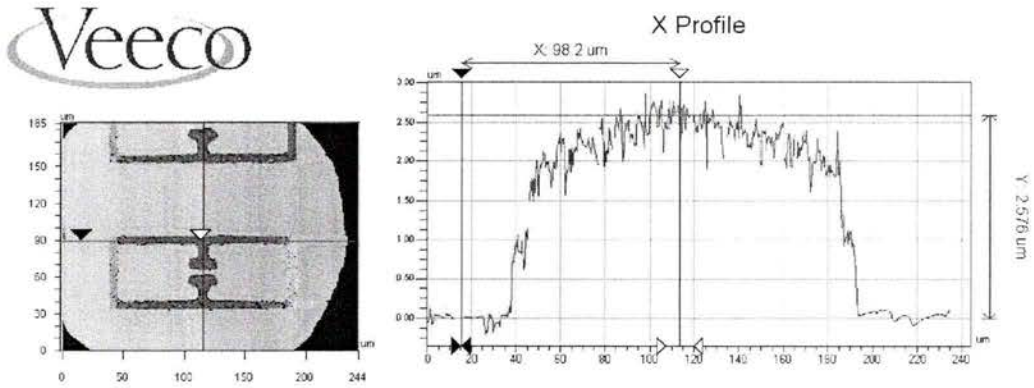

Figure 4·4: 2D profile, x axis projection of the structure at 3V applied

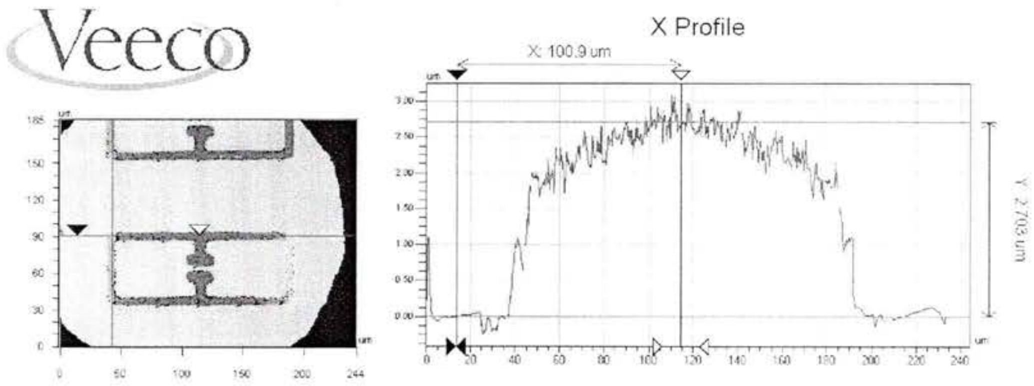

Figure 4·5: 2D profile, x axis projection of the structure at 4V applied

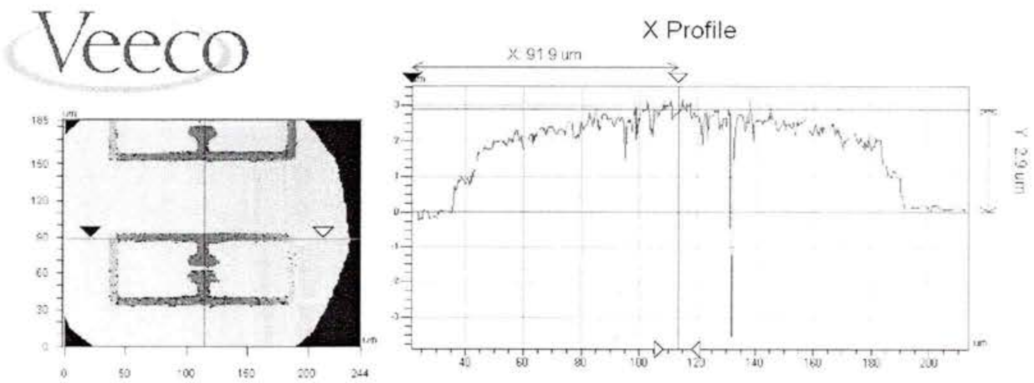

Figure 4·6: 2D profile, x axis projection of the structure at 5V applied

4.2 Terahertz Time Domain Spectroscopy

4.2.1 THz Time Domain Spectroscopy Setup

Terahertz Time Domain Spectroscopy (THz TDS) provides real and imaginary parts of the effective dielectric response which make it possible to reconstruct the signal after passing through a sample.

An 800 nm, 50 fs optical beam is split into two parts with a beam splitter. These beams follows two different pathes. The femtosecond laser goes through a delay stage, other pass through a rectification stage which delivers about a 1 ps THz signal. The femtosecond laser is used for sampling THz signal. Transmitted signal from the sample and the beam coming from delay stage, intersect on a photoconductive detector which transform the optical signal into electrical one (Lee, 2009) Fig.4·7.

During this process THz electric field is measured by using bare substrate as a reference. It is crucial to use identical substrate with the one the sample is built on. A time domain transmission data is obtained and after a fourier transformation of time domain data amplitude and phase information of the transmission is extracted. Dividing sample data by bare substrate (reference), transmission $t(v)$ and phase change $\Delta\phi$ with respect to frequency is obtained for metamaterial (Chen and O'Hara, 2008).

The transmission of our device has been measured at different DC voltages, applied on the device. In other words, electromagnetic output, corresponding to different applied input voltages, is obtained.

4.2.2 Measurement Result

This measurement is conducted at ambient temperatures and atmosphere pressure. A DC voltage is applied across the device (0-6V) and the THz transmission is measured for each voltage increment. The following figures show the frequency

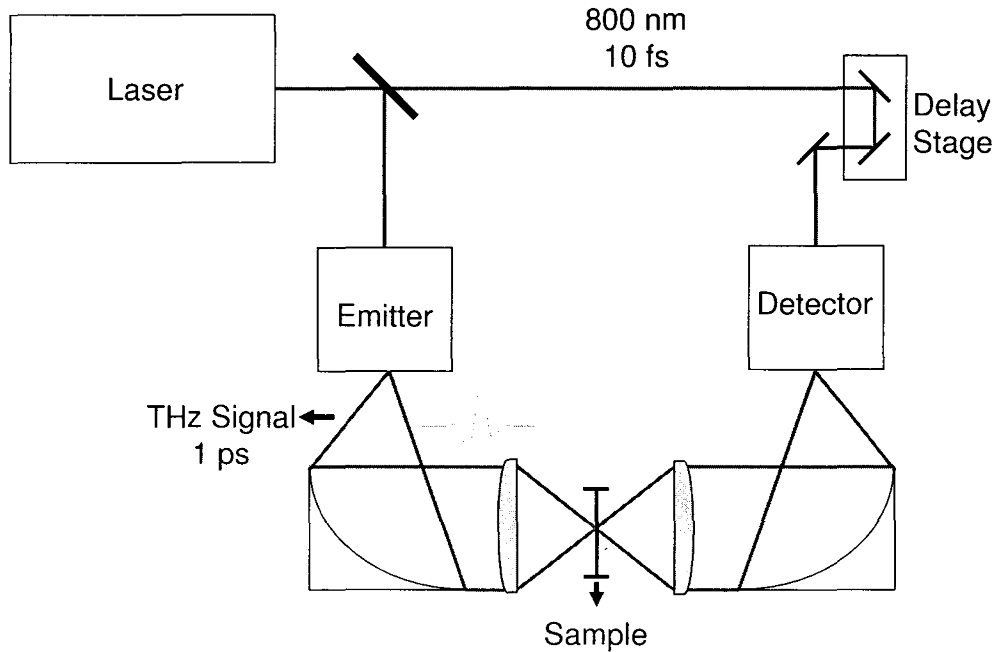

Figure 4·7: THz Time Domain Spectroscopy Setup

shift by increasing voltage over the device. The lower figure is a close up graph for the upper one Fig.4·8.

As it is explained in previous sections current will change the distance between the capacitor plates and the substrate. This measurement shows that our assumption and calculations about resonance frequency change due to electrothermal heating is accurate.

A 6 GHz resonance shift is observed. This is lower than we see in simulations. The possible mechanical reasons are explained in the previous section. In addition to those; electromagnetic simulation bring some differences as well. The main effect comes from geometry. In CST we use a straight structure, raising up from the substrate. However in reality there should be a curvature on the device. Due to the computational cost of curved structure in CST, we avoid this kind of geometry.

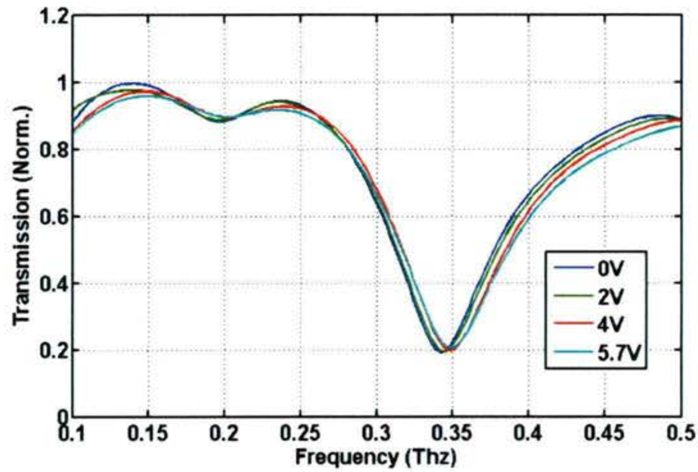

(a)

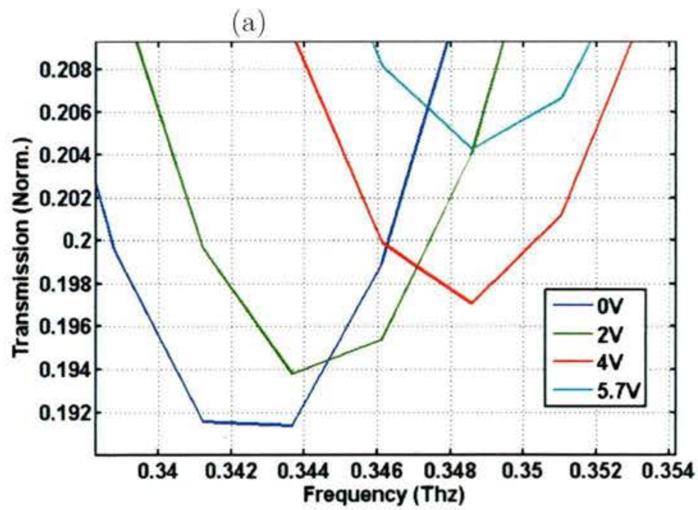

(b)

Figure 4·8: Resonance Frequency Tuning of ETAMM by applied voltage: (a) 0 – 0.5 THz Range; and (b) Close-up graph of the view 1. Around 6 GHz resonance shift

References

Baena, J., Bonache, J., Martin, F., Sillero, R., Falcone, F., Lopetegi, T., Laso, M., Garcia-Garcia, J., Gil, I., Portillo, M., and Sorolla, M. (2005). Equivalent-circuit models for split-ring resonators and complementary split-ring resonators coupled to planar transmission lines. *IEEE Transactions on Microwave Theory and Techniques*, 53(4):1451 – 1461.

Caloz, C. and Itoh, T. (2006). *Electromagnetic Metamaterials Transmission Line Theory and Microwave Applications*. Wiley-Interscience, 1 edition.

Chen, H.-T. and O'Hara, J. F. (2008). Experimental demonstration of frequency-agile terahertz metamaterials. *Nature Photonics 2*, pages 295 – 298.

Chen, H.-T., Padilla, W. J., Zide, J. M. O., Bank, S. R., Gossard, A. C., Taylor, A. J., and Averitt, R. D. (2006). Active terahertz metamaterial devices. *Nature*, 444:597–600.

Chen, H.-T., Padilla, W. J., Zide, J. M. O., Bank, S. R., Gossard, A. C., Taylor, A. J., and Averitt, R. D. (2007). Ultrafast optical switching of terahertz metamaterials fabricated on eras/gaas nanoisland superlattices. *Optics Letters*, 32(12):1620–1622.

Chiao, M. and Lin, L. (2000). Self-buckling of micromachined beams under resistive heating. *Journal of Microelectromechanical Systems*, 9(1):146 –151.

Incropera, F. P. and De Witt, D. P. (1990). *Introduction to Heat Transfer*. John Wiley.

James M. Gere, B. J. G. (2009). *Mechanics of Materials*. Cengage Learning, Toronto, Canada.

Jones, R. M. (2006). *Buckling of Bars,Plates and Shells*. Bull Ridge Publishing, Virginia.

Katsarakis, N., Konstantinidis, G., Kostopoulos, A., Penciu, R. S., Gundogdu, T. F., Kafesaki, M., Economou, E. N., Koschny, T., and Soukoulis, C. M. (2005). Magnetic response of split-ring resonators in the far-infrared frequency regime. *Optics Letters*, 30(11):1348–1350.

Konishi, Y. (1998). *Microwave Electronic Circuit Technology*. CRC Press.

Lee, Y.-S. (2009). *Principles of Terahertz Science and Technology.* Springer Science, LLC.

Marques, R., Ferran, M., and Sorolla, M. (2006). *Metamaterials with Negative Parameters.* Wiley-Interscience, 2 edition.

McCarthy, M., Tiliakos, N., Modi, V., and Frchette, L. G. (2007). Thermal buckling of eccentric microfabricated nickel beams as temperature regulated nonlinear actuators for flow control. *Sensors and Actuators A: Physical*, 134(1):37 – 46. International Mechanical Engineering congress and Exposition 2005 - IMECE 2005, American Society of Mechanical Engineering International Mechanical Engineering Congress and Exposition.

Padilla, W. J., Taylor, A. J., Highstrete, C., Lee, M., and Averitt, R. D. (2006). Dynamical electric and magnetic metamaterial response at terahertz frequencies. *Physical Review Letters*, 96(10):107401.

Paul, O., Imhof, C., Lägel, B., Wolff, S., Heinrich, J., Höfling, S., Forchel, A., Zengerle, R., Beigang, R., and Rahm, M. (2009). Polarization-independent active metamaterial for high-frequency terahertz modulation. *Optics Express*, 17(2):819–827.

Pendry, J., Holden, A., Robbins, D., and Stewart, W. (1999). Magnetism from conductors and enhanced nonlinear phenomena. *IEEE Transactions on Microwave Theory and Techniques,*, 47(11):2075 –2084.

Saleh, B. E. and Teich, M. C. (2007). *Fundamentals of Photonics.* Wiley-Interscience, 2 edition.

Schurig, D., Mock, J. J., and Smith, D. R. (2006). Electric-field-coupled resonators for negative permittivity metamaterials. *Applied Physics Letters*, 88(4):041109.

Smith, D. R., Padilla, W. J., Vier, D. C., Nemat-Nasser, S. C., and Schultz, S. (2000). Composite medium with simultaneously negative permeability and permittivity. *Physical Review Letters*, 84(18):4184–4187.

Veselago, V. (1968). The electrodynamics of substances with simultaneously negative values of ε and μ. *Soviet Physics Uspekhi*, 10:509–514.

Curriculum Vitae

Mehmet Saadeddin OZTURK